4

Ray Tracing work performed

In this chapter, a detailed investigation of ray tracing method carried out for the heliostat field by adopting distribution on the ground as discussed in section 3.5. Although it is favored to spread the heliostats at ground level, while positioning them close to the ground usually provides a dusty atmosphere and other operational inconvenience. To reduce effect of dust settling on the heliostats and accordingly the cleaning necessity, it was proposed to keep the heliostats at an elevated height of 1.5 meter from ground and as carried out in this work.

Solar position coordinate [64,70,71] explicitly calculated in spherical polar-coordinates (point (r,θ,φ) in Cartesian form (x,y,z) for a given hour, which is treated as source. We introduce required angular tilt and required dimension in Eq.12.2 to the source by considering it as a origin and ensure that it strikes the first heliostat kept on ground, which is uniformly illuminated. To illuminate a large number of heliostats spread over a designed field, the extend of the source was increased. The ray density employed this work ranging from 25 rays/m^2 −100 rays/m^2

The necessity of curvature on the Heliostat and its tilt is to nullify/minimize astigmatism and spherical aberration. The effects lead to spread/broadening of the focal spot on the receiver. [142]

4.1 Solar angles and Shadow map

4.1.1 Solar Angles

As mentioned in section 1.7, solar angular position calculation is a prior requirement for high optical efficiency for solar thermal energy generation work. Fig 4.1 show a comparison between the solar angle calculations based calculation from section 2.1 and data from National Oceanic and Atmospheric Administration NOAA [143]

		Elevation angle			Azimuth angle		
Date	Time	Thesis Calculation	NOAA Calculation	% difference	Thesis Calculation	NOAA Calculation	% difference
	900	31.33	31.48	-0.48	104.73	104.22	0.49
	1200	63.66	64.08	-0.66	155.15	154.51	0.41
2703	1600	36.92	37.31	-1.06	251.26	251.79	-0.21
	900	40.35	40.18	0.42	80.75	80.69	0.07
	1200	80.47	80.28	2.24	105.6	105.22	0.36
2706	1600	44.77	45.01	-0.54	277.64	277.54	0.04
	900	32.1	32.33	-1.72	111.68	110.33	1.21
	1200	60.36	61.36	-1.66	165.72	164.69	0.62
2709	1600	31.27	32.06	-2.52	248.97	249.8	-0.33
	900	17.48	17.58	-0.57	128.16	128.23	-0.07
	1200	39.55	39.57	-0.05	168.36	168.45	-0.05
2712	1600	20.58	20.59	-0.04	228.96	228.93	0.01

Table 4.1 : Twelve cases may be considered in this regard as above

In fig 4.1, the thesis calculation is shown as an evaluative comparison with NOAA data [143]. Difference (less than 0.5 % usually) happen because of calculations being Gregorian/ Julian calendars [144] considered in this work and NOAA calculation being from astronomical data. As per literature, the algorithms of calculation vary in processing complexity, precision, and validity time. The maximum errors of these algorithms vary from $0.0003^0$to unit of degrees[145].

4.1.2 Shadow mapping

One of the most influential of the losses in this field of work is that of Shadow formation on ground. Following the angular solar motion throughout the day, the shadow changes its position and the x y positions on ground were calculated for one square meter object i.e a single Heliostat is shown in figure 4.1

This space is left blank

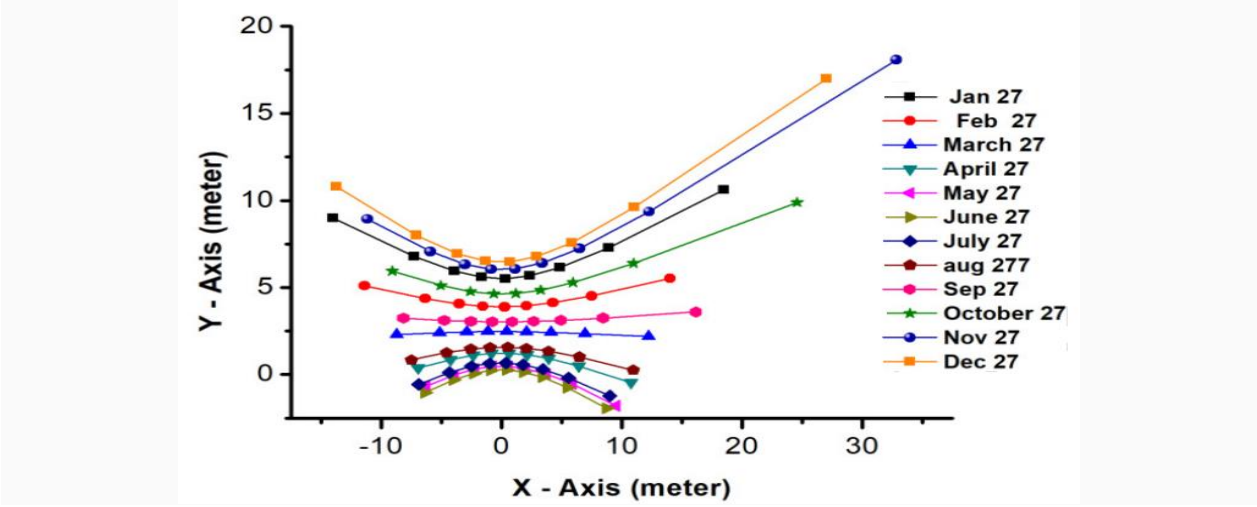

Fig 4.1 Shadaw Map

In this work, heliostats of multiple sizes were designed and the accordingly the positional coordinate (x,y) changes. The nature of the plot however remains intact.

The two factors that affect the shadowing in a given heliostat fields are below. They are:

A. Heliostats on the ground cast shadows one on the another and
B. Receiver or Secondary collectors (in case of Beam Down Optical work) cast shadow on the ground.

The size and position of the shadow depend on the size of the shadow forming element together with solar position (azimuth/altitude). Shadow forming physics is relevant as it has an effect on the usage of the available land area for productive solar thermal resource purpose. For instance, as in Fig 4.1 and will be further discussed in section, November show the maximum shadow area on ground.

4.1.3 Typical Meteorological Year (TMY) and Daily Normal Irradiance (DNI)

TMY is a collection of weather data for a specific location. It lists hourly values of solar radiation (DNI) and other meteorological data for a one-year period. Data for TYI are selected so that it may represent the range of weather phenomena for the location considered and gives the annual averages that are consistent with the long-term averages for the location considered [145].

Direct Normal Irradiance (DNI) data at close intervals of time are essential for the calculation of energy generated by Concentrated Solar Power (CSP) plant. In this work for the calculation of power incident on the receiver and to perform a comparative study, DNI and TMY data [146] were used.

4.2 Beam up configuration

For this investigation, the heliostats were laid on ground with multiple configurations. As the name suggests, solar radiations are incident on heliostats and reflect them to a receiver kept at the top of the tower.

4.2.1 Generation of 100-150 kW optical power

Each heliostats of area (2.5 meter x 2.5 meter) 6.25 m^2 and 50 in number were placed on ground (1.5 m above) with the tower height being 18 m. The first row was placed at 18 m [146] from the receiver foot as per RS pattern as discussed in chapter 3. All the heliostats in this set were made curved as per calculation mentioned earlier and tilts were introduced. The rays, on concentration generated a spot on a receiver of size 1 m^2.Area of the field occupied on ground together with the receiver position was 1192.34 m^2 with rim angle being 10.75^0 .

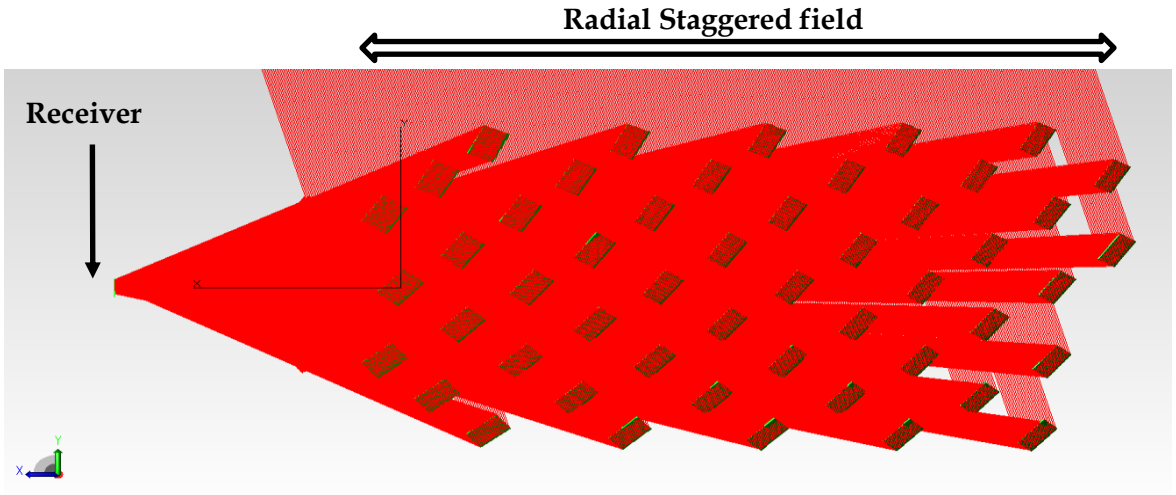

Fig 4.2 : Ray tracing for a field to generate 100 kw power

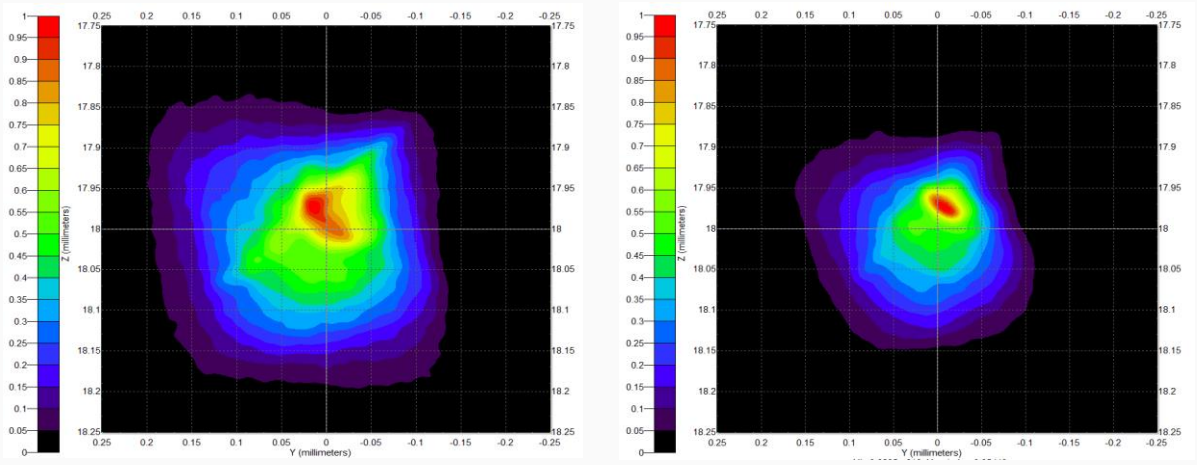

Fig 4.3 show the flux mapping for 2703 1100 hrs and 2709 1100 hrs.

Below is a working simulated data set column-wise for six months and five times each month.

.

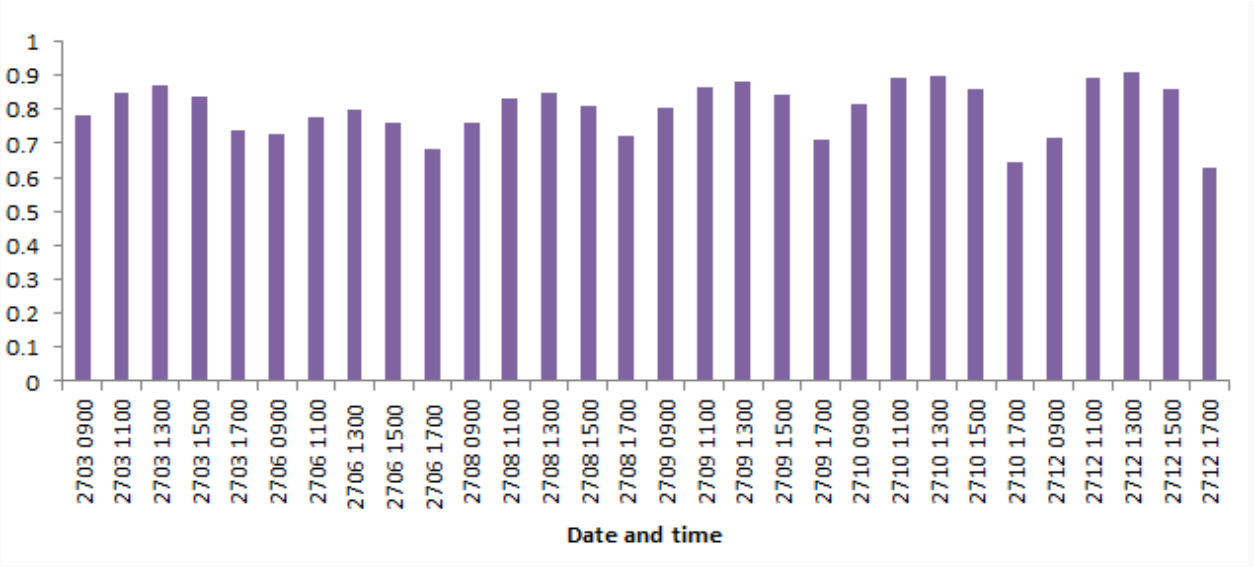

Fig 4.4 Flux wise efficiency vs date/time bar diagram

In fig 4.4, date wise, show that June as the working month is least efficient for power generation whereas October is the best. The distance between the foot of the tower and the first row of heliostat was kept identical to the height of tower at 18 meter [147,148].

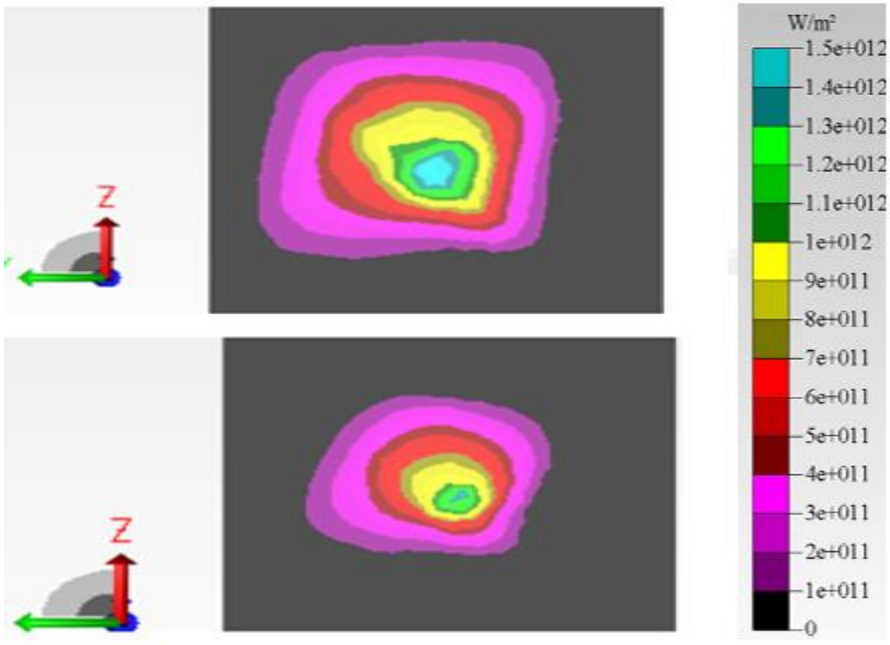

Fig 4.5 Flux map of area vs. Irradiance level

Fig 4.5The 2D Irradiance mapping of the incident irradiance on the surfaces of concern and show the color band according to wavelength in form of color [Tracepro]

Date	Time	Ray wise efficiency	Avg DNI over the working Hours	Power on receiver (kW)
	900	0.822		88.28
	1300	0.915		98.26
2703	1700	0.777	343.6	83.47
	900	0.765		87.07
	1300	0.841		95.71
2706	1700	0.712	364.21	81.58
	900	0.8		62
	1300	0.896		69.22
2708	1700	0.76	247.9	58.84
	900	0.846		132.95
	1300	0.926		145.5
2709	1700	0.748	502.67	117.54
	900	0.859		143.36
	1300	0.948		158.26
2710	1700	0.681	534.23	113.67
	900	0.755		116.51
	1300	0.956		147.68
2712	1700	0.663	494.07	102.33

Table 4.2 : Average power for 100-150 kW heliostat field

As mentioned from analysis of fig 4.5, October in Table 4.2 turns out to be the best month energy generation wise.

Date	Time	Ray wise efficiency	Cosine efficiency	Flux efficiency on receiver
2703	900	0.822	0.82	0.78
	1300	0.915	0.91	0.87
	1700	0.777	0.78	0.73
2706	900	0.765	0.76	0.72
	1300	0.841	0.84	0.8
	1700	0.712	0.71	0.68
2708	900	0.8	0.8	0.76
	1300	0.896	0.89	0.85
	1700	0.76	0.76	0.72
2709	900	0.846	0.85	0.8
	1300	0.926	0.93	0.88
	1700	0.748	0.75	0.71
2710	900	0.859	0.88	0.81
	1300	0.948	0.95	0.9
	1700	0.681	0.81	0.64
2712	900	0.755	0.88	0.71
	1300	0.956	0.96	0.91
	1700	0.663	0.85	0.63

Table 4.3 Normalized ray efficiency factors for 100-150 kW heliostat field

4.2.2 Generation of 1.4 MW optical power

For this specific design, 40 Heliostats of size 64 m^2(8 meter x 8 meter) each were used making the total reflective area to be 2560 m^2 and the height of the tower was kept at 25 m. The length of the field was 157 m , breadth was 55.6 m making the area occupied on ground to be 6256 m^2 and the rim angle being 16.62^0.The size of the receiver, square in shape, was 16 m^2. The heliostats were curved and tilted to achieve higher concentration.

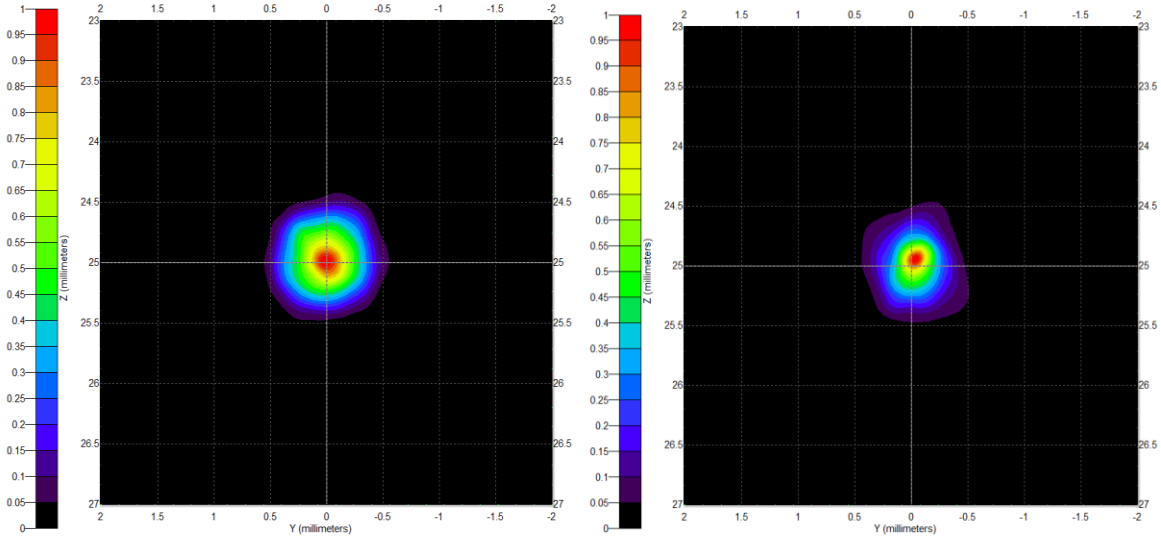

Fig 4.6 show the flux mapping for 2703 1100 hrs and 2709 1100 hrs.

The distance between the foot of the tower and the first row of heliostat kept at 25 m[13]. The field was made Radial Staggered and following are the efficiency factors obtained.

Date	Time	Ray wise Efficiency	Cosine efficiency	Flux efficiency on receiver
2703	900	0.709	0.79	0.672
	1300	0.788	0.88	0.748
	1700	0.713	0.76	0.676
2706	900	0.658	0.72	0.624
	1300	0.721	0.8	0.683
	1700	0.617	0.67	0.584
2708	900	0.7	0.77	0.664
	1300	0.775	0.85	0.736
	1700	0.637	0.73	0.604
2709	900	0.775	0.82	0.687
	1300	0.764	0.89	0.753
	1700	0.633	0.77	0.6
2710	900	0.702	0.85	0.665
	1300	0.804	0.92	0.763
	1700	0.545	0.79	0.516
2712	900	0.602	0.86	0.572
	1300	0.807	0.93	0.765
	1700	0.454	0.83	0.429

Table 4.4 : Normalized efficiency factors 1.4 MW

Table 4.4 show the efficiency factors of this configuration of work. March turns out to be the most efficient month.

4.2.3 Heliostat field as cornfield layout

The basic idea for the heliostat field layout design is to locate the receiver and the heliostats in a given position on land [149]. The placing of the heliostats was done on the ground in a similar fashion as the corns are thrown for plantations.

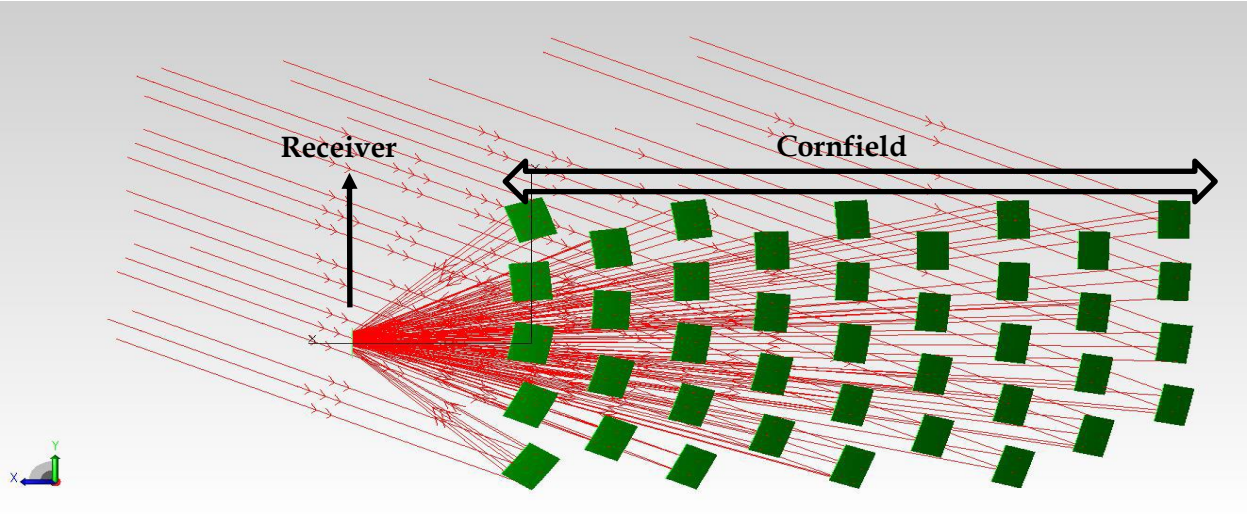

Fig 4.7 Cornfield on the ground directing the solar radiation to the receiver.

In Cornfield design as in section 3.5.2 and mathematics of Eq 6.3 was used for design on the field with the heliostat size to be 5 X 5 and buffer distance being kept as unity. For this field design the row and column spacing were kept, by calculation, as 8.07 units. In all, 40 Heliostat were placed on field.

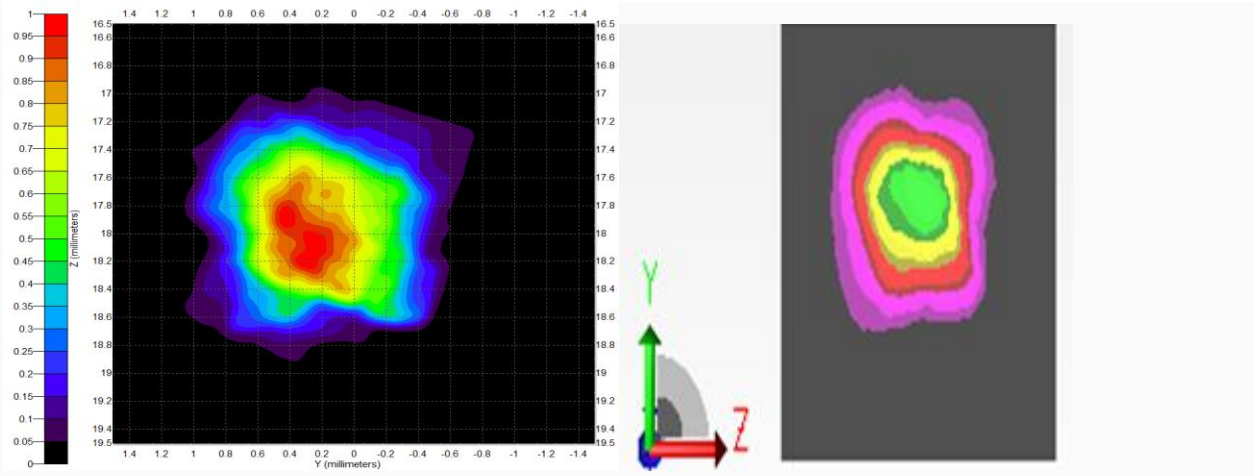

Fig 4.8 show the flux mapping normalized (left) and 2D irradiance plot 2706 1200 hrs .

Date	Time	Cosine Efficiency	Ray efficiency	Flux efficiency
2703	900	0.83	0.686	0.645
	1200	0.92	0.726	0.688
	1600	0.86	0.65	0.686
2706	900	0.75	0.641	0.608
	1200	0.84	0.719	0.683
	1600	0.77	0.659	0.625
2709	900	0.85	0.685	0.649
	1200	0.94	0.727	0.689
	1600	0.86	0.66	0.625
2712	900	0.9	0.631	0.593
	1200	0.98	0.719	0.677
	1600	0.92	0.665	0.628

Table 4.5: Cosine, ray and flux wise normalized efficiency for cornfield design

The receiver in this configuration was kept as 3 meter x 3 meter at a target height of 18 meter. The field area for this configuration was 2373 m^2.

4.2.4 Estimation and optimization of heliostat field for 400 kW to 550 kW optical power using ray tracing method .

Heliostat field layout, as per power generation is concerned, is dependent on estimation of a set of existing data and perform a set of iteration to optimize the field particulars.

In this work, to begin the estimation, heliostats of the size (4 meter x 4meter) 16 m^2 and (5meter x 5 meter) 25 m^2 were utilized to generate a working field with the target of power generation was 400 kW and 550 kW respectively [149].

A flat mirror has the advantage of relatively cheap construction, and the intrinsic capability to host multiple experiments. Additionally, in comparison to a convex mirror, there is significantly less optical distortion of the solar energy collected on a solar receiver at the top of a tower .

As mentioned in Fig. 4.20, the size of the field was 3000 m^2 and 4000 m^2 (approx.) respectively which made the field to reflective area ratio as 3.75 and 4 respectively.

This study was important and relevant as according to literature Heliostat field design cost involves 40% of the total cost of (keeping all other cost factors insignificant) of solar thermal plant development.

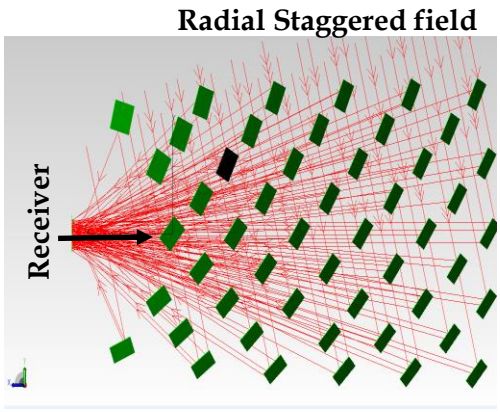

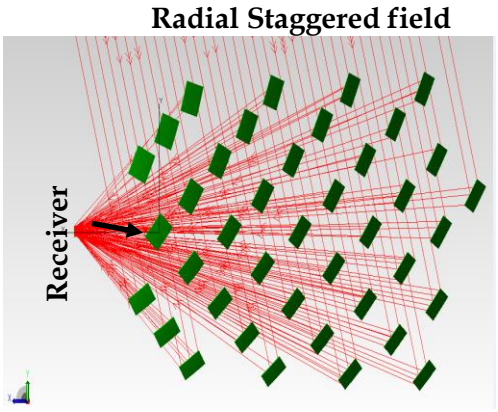

Fig 4.9 (a)RS field for 4 x 4 (50 in number)

Fig.4.9 (b) RS field 5 x 5 (40 in number)

Although in this work, the Heliostats are directed to take the rays to the receiver, the Heliostats were not curved and hence rays are incident on the receiver but not focused. Here heliostats were considered of two dimensions namely 4 x 4 and 5 x 5 and studied in a comparative manner. The field size on the ground was 2313 m^2 (rim angle 12.6^0) for 4x4 Heliostats and 2889 m^2 (rim angle 14.62^0) for 5 x 5 heliostats.

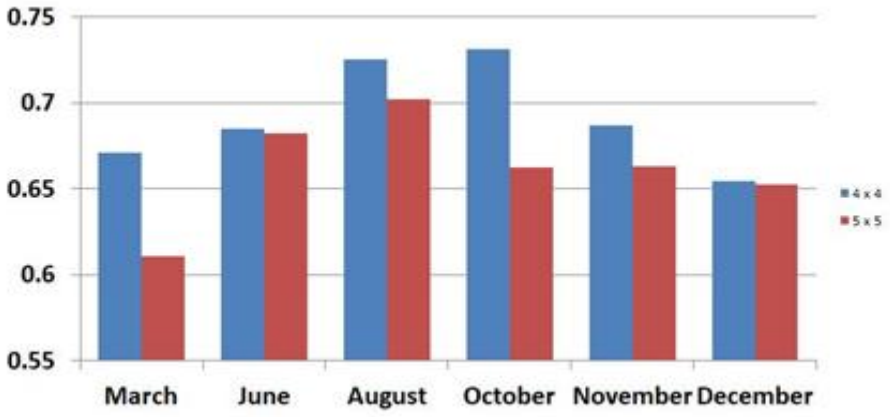

Fig. 4.10: Average ray wise efficiency on the receiver for two mentioned field.

As the work of Solar thermal power generation has to consider the transient behavior of solar radiation in a quantitative sense, it is necessary to estimate the power that is incident on a particular day and time to optimize it for some other time.

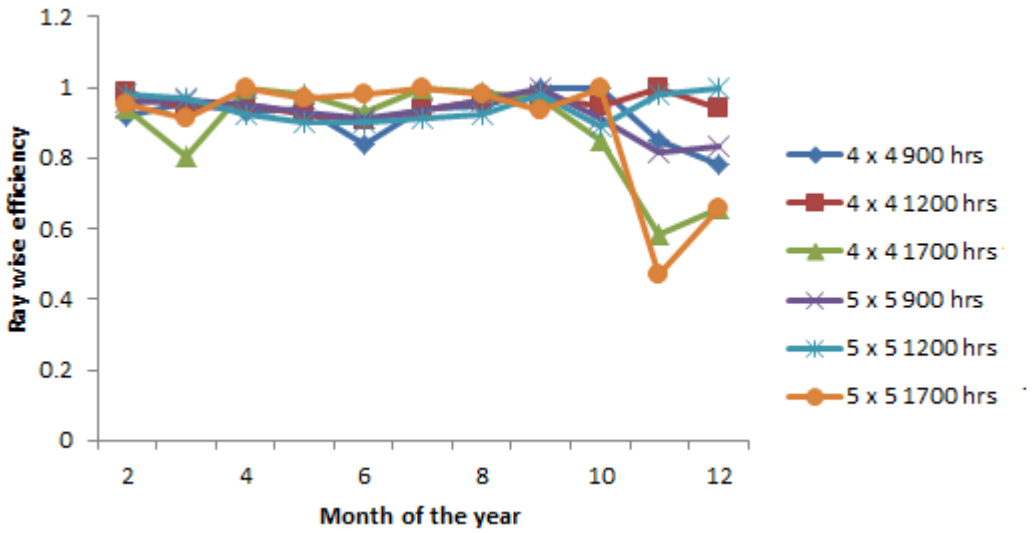

Fig.4. 11 : Ray wise efficiency on the receiver for two mentioned field and three chosen Hours os work i.e 0900 hrs ,1200 hrs,1700 hrs

Fig 4.11 and Fig 4.13 are supplementary to each other which show that November poses the maximum inefficiency due to Shadow and hence the shadow area on ground is the maximum. Accordingly, Fig 4.11 reflects least number of rays (normalized) to the receiver.

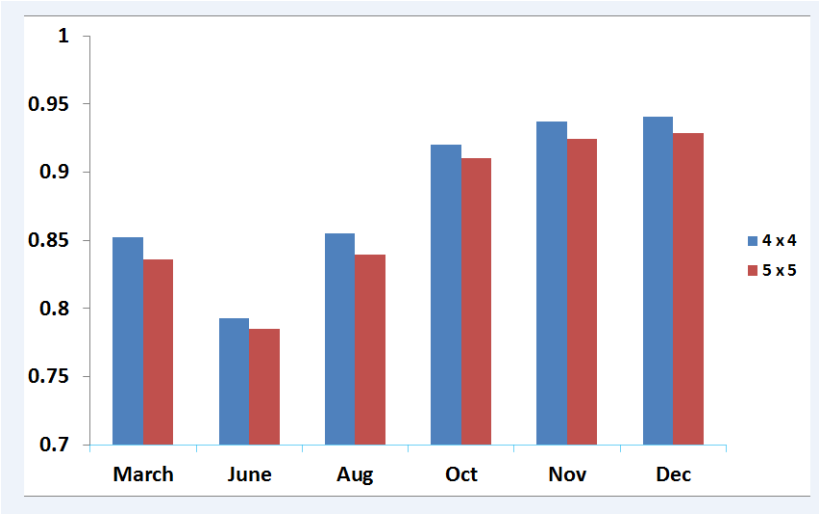

Fig 4.12 Normalized cosine efficiency for chosen months as an average of working hours

Shadow of the heliostats on the field is considered as one of the biggest loss controbuting factor together with other. In this particular work, the shadow that a single Heliostat casted on others was considered. Fig 4.13 depicts the shadow diagram on the ground. The said figure is a Month vs. area of shadow on ground map which show that November has the largest shadow on ground. The Heliostats in both the mentioned cases was 5 meter x 5 meter.

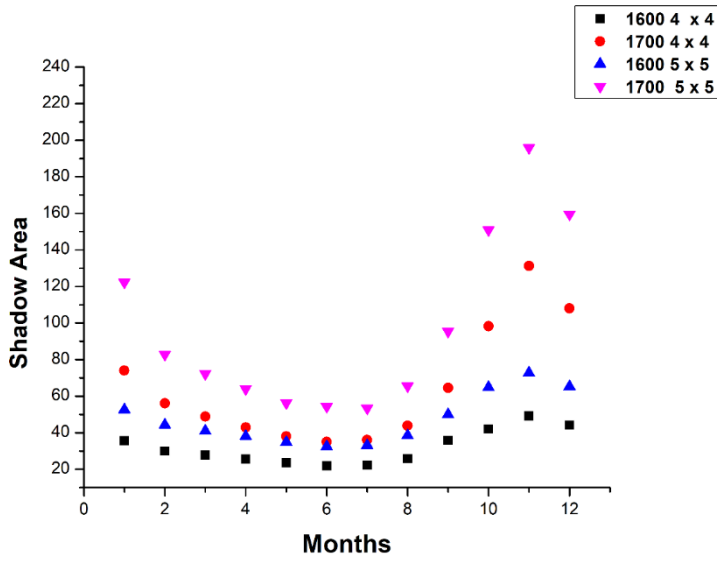

Fig.4.13 Shadow area on the ground for heliostat sizes 16 m² and 25 m²

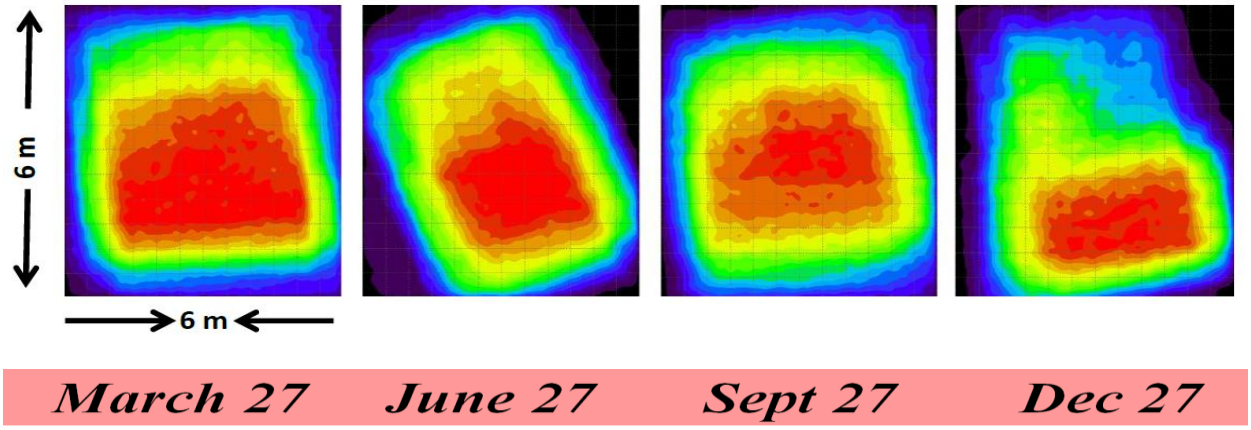

Fig 4.14 Flux map on receiver for 5 m x 5 m at 900 hrs

In figure 4.14, flus map on the receiver for four chosen days, as mentioned, at 0900 hrs are shown. The days were chosen as nearing the Equinoxes and the Solstices. Fig 4.11 (November having least ray efficiency), Fig 4.13 (November having maximum shadow area on the ground) confirm that November casts largest shadow for 5x5 heliostats. Further, as in Fig 4.14 ,December has the most faint flux map which show least number of rays (among four concerned month) are incident in December (nearing November).

Time (hrs)	Layout Design		Total reflective area(m^2)	Total area of field (m^2)	Ray efficiency (Normalized)	Cosine efficiency	Total ooptical power on receiver (kW)
	Radial Spacing (m)	Azimuthal Spacing (m)					
1600	11.36	9.39	800	2987	0.707	0.8504	
	13.39	11.64	1000	3886	0.685	0.8135	
1700	11.36	9.39	800	2987	0.6358	0.765	
	13.39	11.64	1000	3886	0.62	0.7617	
27-Aug	11.39	9.39	800	2987	0.725	0.725	3190
27-Aug	13.39	11.64	1000	3886	0.707	0.707	3861

Table 4.6 : Estimation of optical power on August 27 for 1600 hrs,1700 hrs and whole day shown in above table

The estimation of power was performed on the basis of Daily Normal Incidence (DNI)[70]

4.2.5 A novel uniform illumination on receivers in central tower systems using ray tracing approach

In this investigation, a novel cavity receiver design was considered for uniform illumination using a circular heliostat field [150]. The cavity receivers are capable of achieving high efficiency because of high light trapping ability and reduced thermal losses [148]. An optical model was integrated with hydrodynamic model along with thermal losses which enable us to simulate a cavity receiver model structure [148,117]. The full design of receiver was configured using a concentrated parabolic concentrator (CPC) is juxtaposed between two hyperboloids to give it a tubular shape in Fig.4.15.

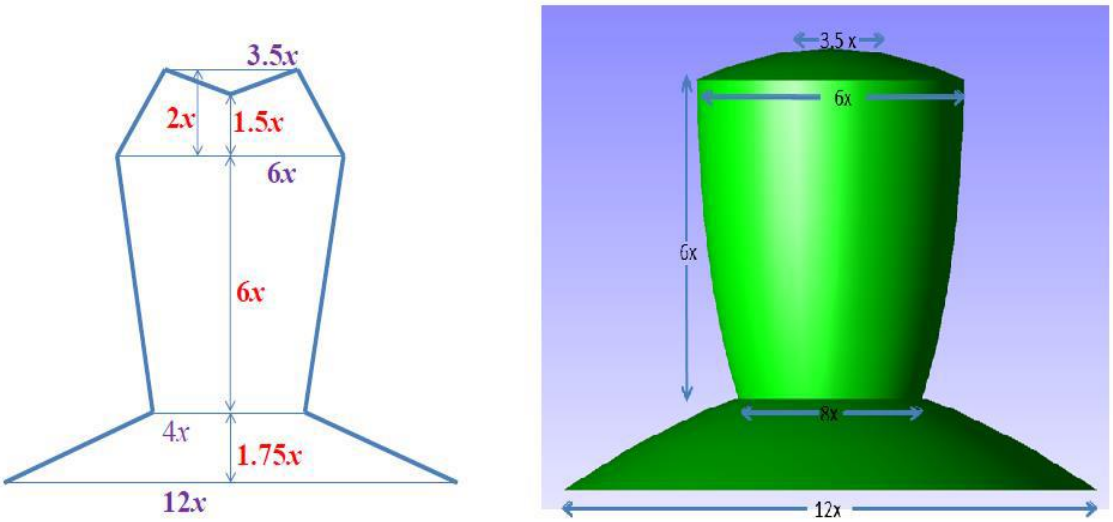

Fig 4.15 Curved receiver setup left: Pictorial,Right : Software wise

A Monte Carlo ray tracing (MCRT) technique was used by employing the receiver system as shownin Fig 4.16 and detailed investigations were done. A spatially-resolved receiver profile was made to simulate as absorption of solar radiation in the cavity taking the account of blocking & shadowing, spillage and reflection losses. Cavity surfaces were assumed to be perfectly absorptive, MCRT would allow us estimate the contribution of both the spatial spread of concentrated flux at the aperture to be simulated.

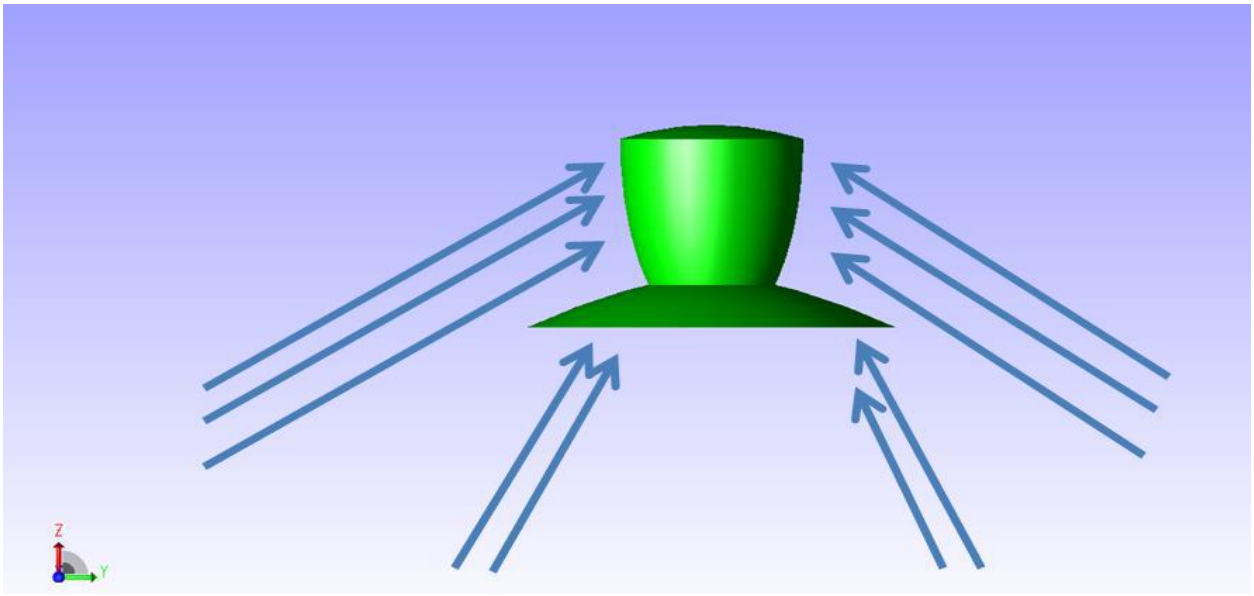

Fig 4.16 Curved receiver being subjected to ray tracing from all sides

To illuminate the designed receiver to work in a highly efficient way, a set of 181 heliostats were placed in a circular pattern was spread on the ground using a well-known radial staggered layout as shown in Fig 4.16 above. Rays from the first two rings consisting 27 heliostat were aimed to hit the interior of the receiver i.e the back of top hyperboloid. Remaining heliostats were targeted to hit the exterior of the device i.e the CPC. Fig 4.17 shows a ray traced simulated picture in which heliostats surrounding the device as mentioned is shown above .

In the specific investigation, two different configuration for the receivers were explicitly carried out with x= 0.2 and x=0.6, as shown Fig 4.16 for heliostats having dimensions 2 m x 2 m and 5 m x 5 m respectively. Figure 4.18 provides normalized rays reaching the receiver on December 27th at an interval of one hour by utilizing the heliostats having dimensions 2 m x 2 m and 5 m x 5 m. Figure 4.19 provides normalized rays reaching the receiver for three operational hours during six different months with having dimensions 2 m x 2 m and 5 m x 5 m.

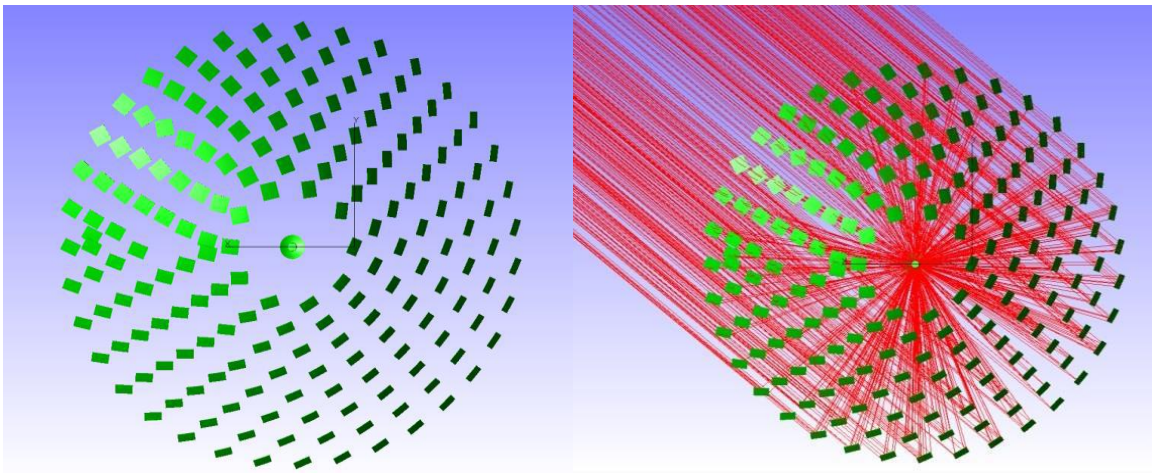

Fig 4.17 Field layout: left: Circular heliostat field, Right : Ray traced circular heliostat field

Fig 4.17 (left) is a design of RS map on the ground with 181 Heliostats and fig.4.17 (Right) is the same map with heliostats curved and tilted (simulated).

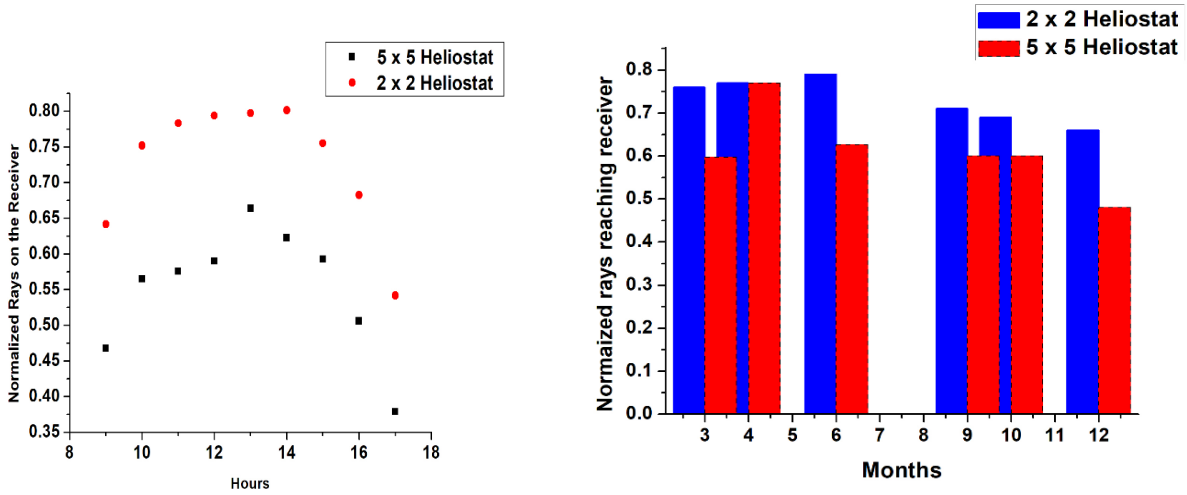

Fig 4.18 above: Normalized number of rays on the receiver obtained by ray tracing on December 27, an one hour interval for two differently sized Heliostats

In the above Fig 4.19, a normalized number of rays on the receiver obtained by ray tracing for six months (randomly) averaged for three hours, with heliostat dimension being 2 m x 2 m and 5 m x 5 m were presented.

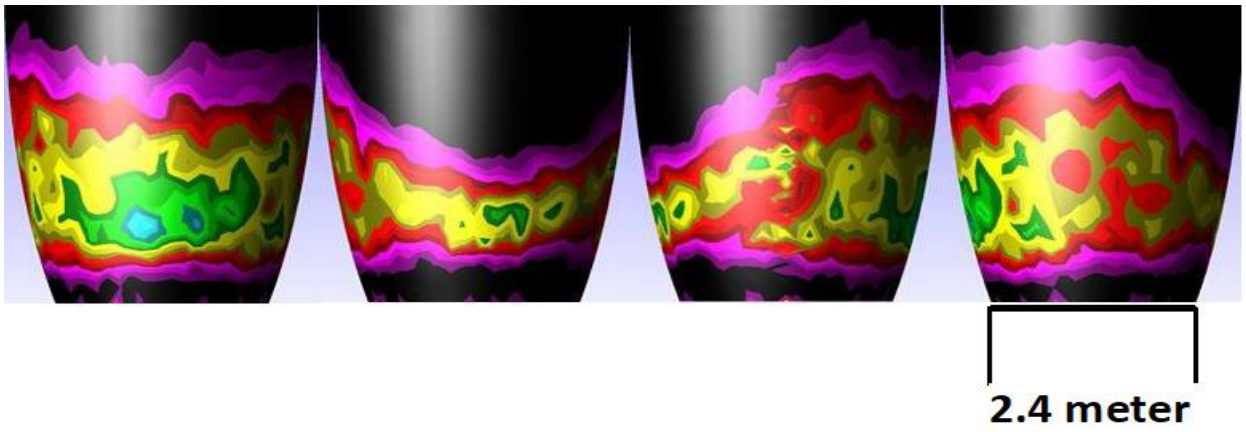

Fig.4.20 3D Flux map on the CPC from all sides

Fig 4.20 above is a 3D flux map for x = 0.6 at 1200 hrs with CPC height being 3.24.

Time (hrs)	Layout Design		Area of single Heliostat (m^2)	Receiver dimension opening (6x) (Refer fig 4.21)	Area of the field (m^2)	Normalized ray efficiency	Total ooptical power on receiver (kW)
	Radial Spacing (m)	Azimuthal Spacing (m)					
1600	7.21	4.89	4	1.2	4070	0.68	
	13.39	11.64	25	3.6	19438	0.506	
1700	7.21	4.89	4	1.2	4070	0.55	
	13.39	11.64	25	3.6	19438	0.38	
27 Dec	7.21	4.89	4	1.2	4070	0.7276	2897.3
(All hrs)	13.39	11.64	25	3.6	19438	0.56	13688.12

Table 4.7 : Total Optical power estimated using ray tracing method for the heliostat dimension of 2 x 2 and 5 x 5 heliostats for Dec 27 (whole day with 1600 and 1700 hrs separately)

0900 Hrs				
Total number of rays on the receiver	Total flux on receiver	Ray wise efficiency on receiver	Flux wise efficiency	Date under consideration
54531	51621	0.482	0.456	Jan-27
61719	58441	0.545	0.517	Feb-27
66036	62618	0.583	0.553	Mar-27
69168	65642	0.611	0.58	Apr-27
69007	64911	0.604	0.573	May-27
68427	64914	0.604	0.574	Jun-27
68845	65311	0.608	0.577	Jul-27
67946	64456	0.601	0.569	Aug-27
66708	63251	0.598	0.559	Sep-27
60258	57040	0.533	0.504	Oct-27
58278	55149	0.515	0.487	Nov-27
52995	50147	0.468	0.443	Dec-27

Table 4.8 Ray and flux wise normalized efficiency on the receiver month wise on a particular day for 5 x 5 Heliostat size and x = 0.6 (Fig 4.21) in the receiver designed at 0900 hrs. It was a study of receiver with x = 0.6 for 0900 hrs in 27th of all month

Hour of day	Ray wise efficiency	Flux wise efficiencu	Month under considerat ion	Average DNI over working hours	Power on Receiver (kW)
900	0.642	0.608			299.39
1000	0.752	0.741			350.7
1100	0.783	0.751			359.34
1200	0.793	0.756			370.36
1300	0.797	0.762			371.93
1400	0.801	0.717			373.71
1500	0.751	0.647			352.27
1600	0.682	0.646			317.41
1700	0.541	0.513	Dec-27	644.29	252.69
900	0.724	0.687			180.14
1200	0.858	0.813			213.42
1700	0.721	0.684	Mar-27	343.6	179.34
900	0.764	0.725			201.52
1200	0.869	0.825			229.23
1700	0.746	0.708	Jun-27	364.23	196.71
900	0.743	0.679			270.31
1200	832	0.767			302.57
1700	0.551	0.557	Sep-27	502.67	200.48
900	0.715	0.678			276.73
1200	0.808	0.767			312.72
1700	0.788	0.557	Oct-27	534.23	227.37
900	0.748	0.709			239.24
1200	0.86	0.816			275.26
1700	0.704	0.668	Apr-27	442	225.28

Table 4.9 :Power on the receiver month wise on a particular day for 2 x 2 Heliostat size and x = 0.2 in the receiver designate at mentioned time.

Reflective area on the above case is =181*4 = 724 m^2

The total rays on the heliostats : 181*4*100 = 72400 (100 rays launched per m^2) with r = 400 in the polar coordinate set.
Value of x for receiver : 0.2

Date under consideration	Hours of work under considerat ion	Ray efficiency	Cosine efficiency	Avg. DNI over the working Hrs (W/m^2)	Power on receive (MW)
	900	0.47	0.71		1.37
	1000	0.56	0.74		1.64
	1100	0.57	0.76		1.66
	1200	0.59	0.77		1.72
	1300	0.67	0.77		1.95
	1400	0.62	0.06		1.81
	1500	0.59	0.75		1.72
	1600	0.51	0.72		1.49
Dec-27	1700	0.38	0.69	644.29	1.11
	900	0.58	0.78		0.9
	1200	0.67	0.81		1.04
Mar-27	1700	0.56	0.73	343.6	0.87
	900	0.6	0.77		0.99
	1200	0.68	0.83		1.12
Jun-27	1700	0.58	0.75	364.23	0.95
	900	0.59	0.59		1.34
	1200	0.68	0.68		1.55
Sep-27	1700	0.51	0.51	502.64	1.16
	900	0.61	0.61		1.48
	1200	0.67	0.67		1.62
Oct-27	1700	0.53	0.53	534.23	1.28
	900	0.74	0.74		1.48
	1200	0.82	0.82		1.64
Apr-27	1700	0.73	0.73	442	1.46

Table 4.10 :Analysis of Heliostatic field with receiver of x= 0.6
Total reflective area for the above design : 4525 m^2,Reflective area size for receiver with x = 0.6

4.2.6 Ray Tracing Approach for the Performance Evaluation of Bladed and Flat-Plate Receiver in Central Tower Systems

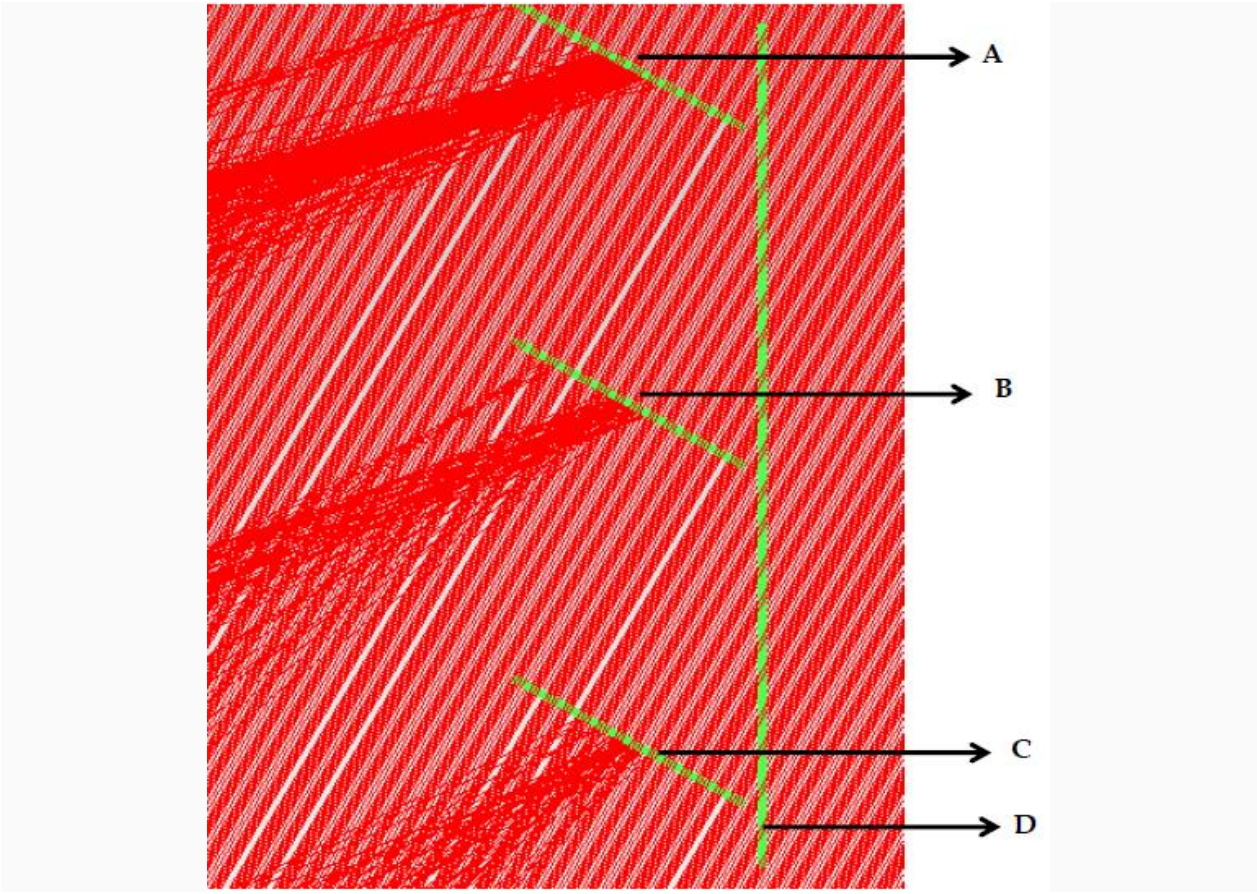

Fig.4.21Bladded receiver A,B,C mounted against a background support of D

An additional investigation in heliostat fields were attempted by introducing a bladed receiver design [151], wherein three blades (receivers) were shown in Figure 4.21 (the blades were A,B,C in Figure 4.21) together with a supporting element (D in above figure). A comparative study between flat receiver and bladed receiver were done in this work with twelve different cases. The heliostats were given specified curvature and tilts to achieve high concentration and to reduce losses. The different positions of the bladed receiver were kept at 16, 20 and 24 meter above the ground and a height of 18 meter was used for the flat receiver. In case of dealing with bladed receivers, with forty (40) heliostats spread on ground, heliostats numbering 22, 10 and 8 were directed to bladed receiver position A, B and C respectively.

Date	Time (hrs)	Ray Wise efficiency		Cosine efficiency		Avg DNI based on working Hrs	Power on receiver (kW)	
		Flat Receiver	Bladed eceiver	Flat Receiver	Bladed eceiver		Flat Receiver	Bladed eceiver
	900	0.708	0.785	0.824	0.807		254.19	281.79
	1300	0.818	0.868	0.913	0.901		298.38	311.54
2703	1700	0.71	0.741	0.808	0.781	358.83	254.77	265.89
	900	0.67	0.718	0.743	0.738		255.52	273.83
	1300	0.768	0.766	0.822	0.83		292.93	292.14
2706	1700	0.662	0.681	0.708	0.706	381.8	252.43	259.91
	900	0.76	0.806	0.832	0.831		392.54	416.51
	1300	0.83	0.845	0.929	0.914		427.09	436.34
2709	1700	0.675	0.703	0.979	0.779	516.5	348.64	363
	900	0.647	0.671	0.896	0.866		370.64	384.38
	1300	0.45	0.864	0.94	0.944		485.57	495.02
2712	1700	0.562	0.878	0.867	0.838	572.68	321.9	330.78

Table 4.11Bladed receiver ray wise efficiency and power generation capacity work as compared to flat receiver work

Table 4.11show increase in the ray efficiency in the bladed receiver as compared to flat receiver for twelve cases round the year. Ray efficiency is calculated as a ratio of number of rays on receiver and number of rays on the Heliostats i.e the collectors. That value together with value of reflective area and the DNI dictates of the value of power generation.

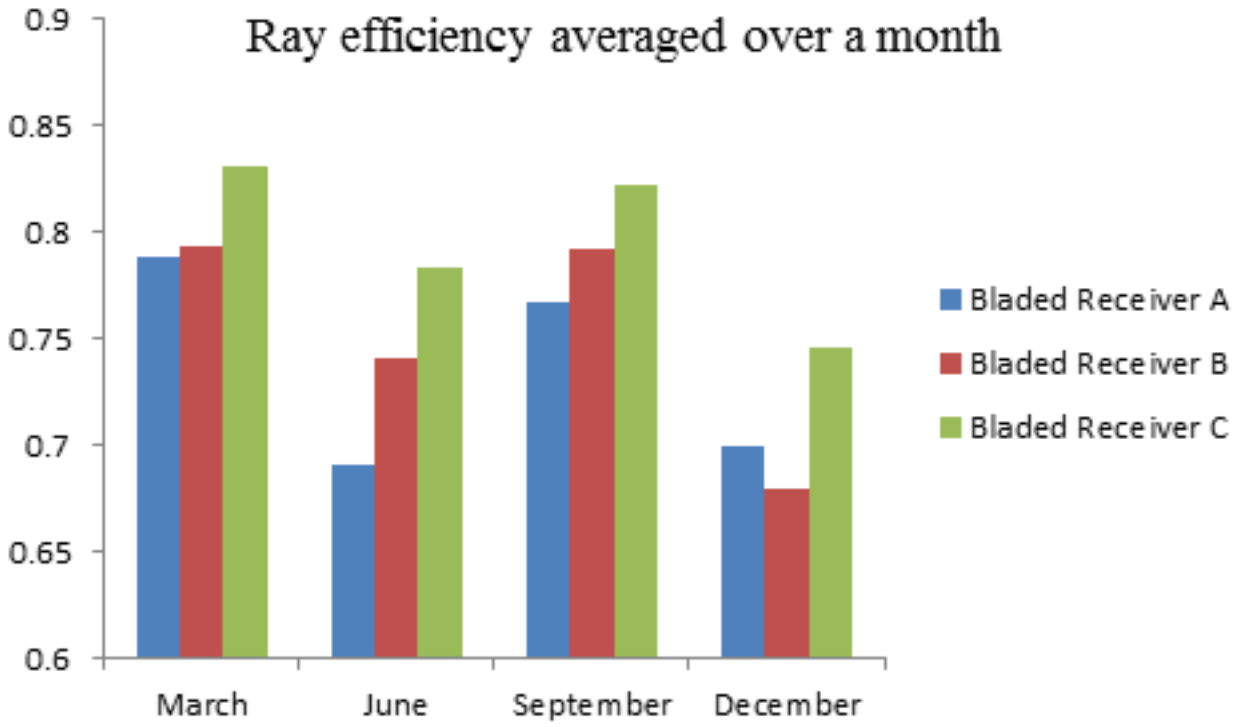

Fig4.22. Ray efficiency individual blade wise over month of study

In fig 4.23 below, individual bladed receiver was considered separately.

The receiver at the lowest position which accepts rays from nearest to the tower was found to be the most efficient.

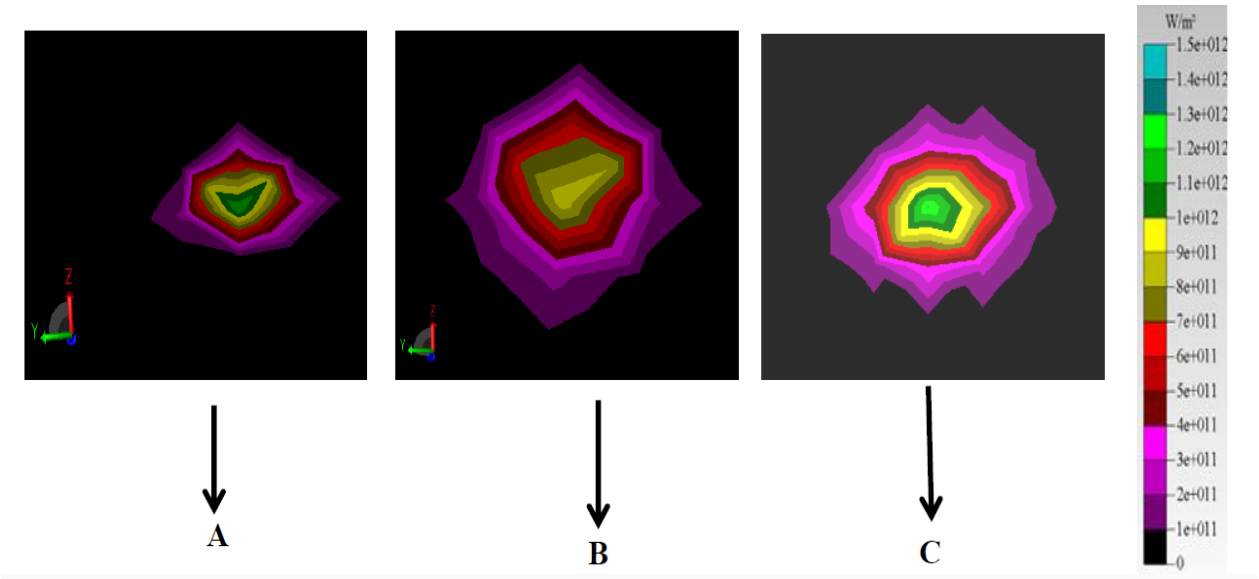

Fig 4.23: 2D illumination of the bladed receiver A, B, C respectively

In Fig 4.23, in a separate fashion shows the 2D immunization on the individual blade.

4.2.7 Sunflower (SF) / Fermat's field design

In the central receiver system (CRS), it has been observed by various investigators [80] that heliostat near the tower contributes to efficiency more than those at a distance. That stands as one of the biggest disadvantages of RS configuration. In a circular field, the density of the heliostat remain the same as in RS field, alternatively sunflower like distribution of heliostats which leads to spiral spread nature of the heliostats and it is capable of getting more heliostats on the ground leads to higher heliostat density. This leads to a tradeoff between usage of available land area and efficiency.

As the Sunflower design is spread spirally on ground, cylindrical receiver is necessary for this design.

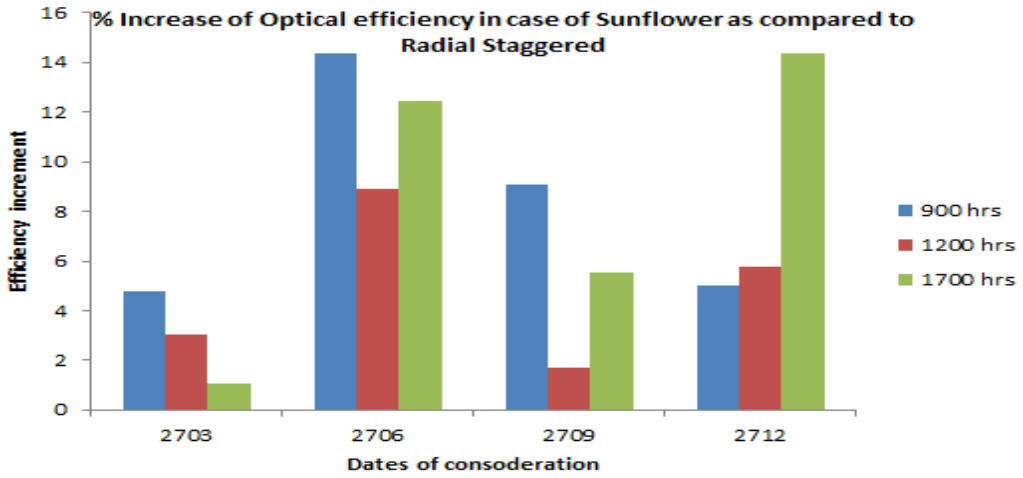

Fig 4.24 : Increased efficiency in case of Sunflower as compared to RS

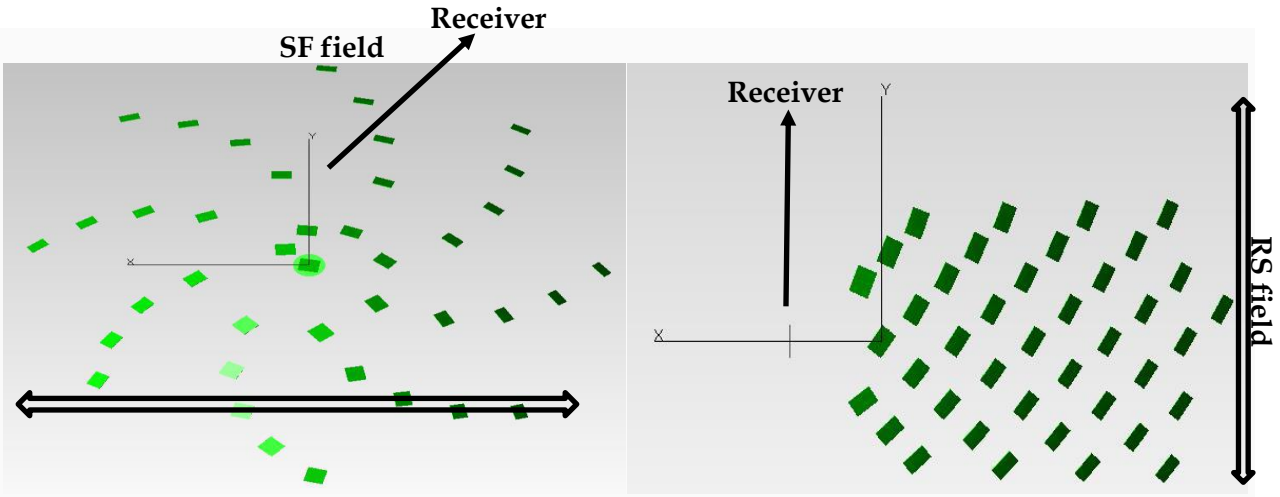

Fig 4.25 Left: Sunflower geometry, Right ; Radial Staggered Geometry

For the purpose of design, an estimation of a practically feasible and implementable of solar field in terms of SF and RS were done to ensure a fair comparison between both algorithms. The solar field layouts resulting from the different algorithms was compared in this simulation work for different scenarios to cover a relatively wide range of days and time wise applications. As shown in Fig 4.35, and for reasons stated above, SF is advantageous in terms of optical efficiency.
In Fig 4.25, a plan wise view of SF and RS fields is shown. Both are designed with 40 heliostats of size 5 meter x 5 meter. In case of RS, geometry in section 3.5.1 and for SF, spiral geometry of section 3.5.3

4.3 Ray tracing methods using beam down optics

In this section, the investigations were done by employing radial staggered field on the ground, while three different configurations were introduced as beam down optics.

4.3.1 Inclined plane as beam down optics

In this way of work, the radiation from the source, after reflection from Heliostats as primary reflector are taken to the Inclined plane which is considered as the secondary reflector [100]. The size of the inclined plane was kept at 26 x 24 m^2. Because of its size, it usually blocks the radiation from source and also causes shadow on ground. To accommodate for that, the first two/three rows of heliostats are not considered for the final calculation. To compensation for this loss and keep uniform number (40) of Heliostats as primary reflector set, extra heliostat rows were added at the back for ray tracing purpose. This loss and hence compensation is depends on solar position which is dynamical quantity.
Also, in this case, to avoid direct illumination to the receiver kept on the ground from the source, an obstruction was positioned, which ensures only reflected ray from heliostats (primary concentrators), further reflected by inclined plane (secondary reflector) reaches the receiver.
Heliostats were all curved and tilted for this purpose of work. In the figure below, y axis is dimensional shortened to 24 m as mentioned to suit the receiver of size 5 meter x 5 meter = 25 m^2 at the ground.

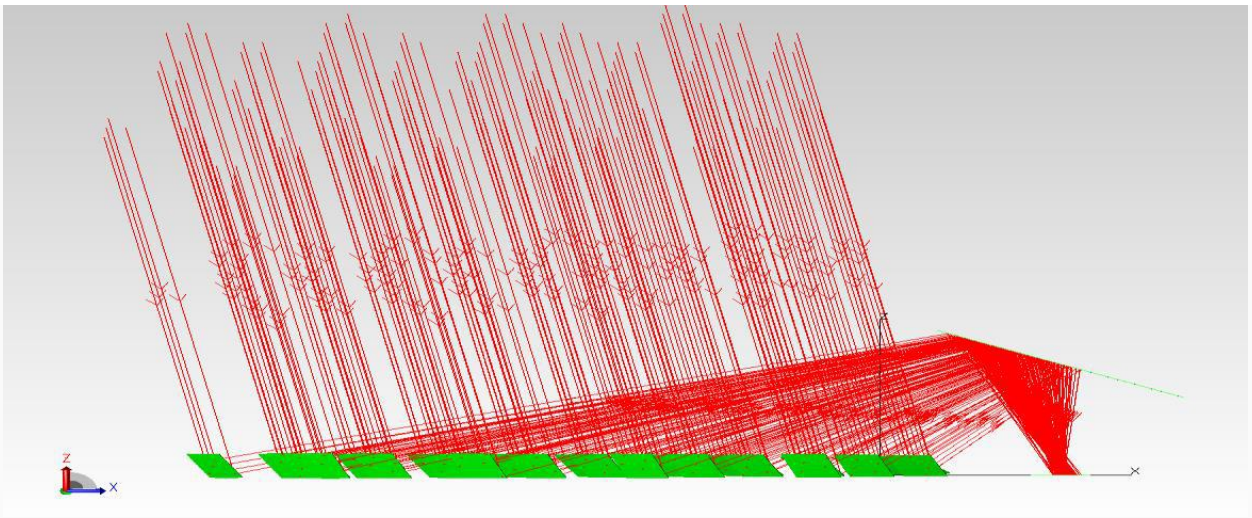

Fig 4.26. Ray tracing with Inclined plane as secondary reflector

Date	Time	Ray wise efficiency on ground
2703	900	0.733
	1200	0.756
	1600	0.709
2706	900	0.667
	1200	0.744
	1600	0.682
2709	900	0.722
	1200	0.752
	1600	0.702
2712	900	0.647
	1000	0.736
	1100	0.752
	1200	0.747
	1300	0.731
	1400	0.714
	1500	0.69
	1600	0.639
	1700	0.573

Table 4.12: Ray wise efficiency for Beam Down with inclined plane

4.3.2 Hyperboloid as a secondary reflector

In case of this work, a hyperboloid of one sheet was used as secondary reflector [89,99,102]. It was placed in a mechanical manner at the position of the higher focal point and accordingly, the rays were launched.

In the design, z-axis is considered to be vertically upwards and the major axis of the hyperboloid of work. The upper focal point i.e the aim point was kept at (18,0,18) and the upper vertex was positioned at (18,0,15.8)

This makes the upper focal distance i.e f_1 = 2.2 m.

The receiver point i.e the lower focal point is the distance between the upper vertex and the lower focal point. The lower focal point with calculation, was kept at **(18, 0.1, 0)** i.e the lower focal distance f_2 was kept at 15.8 m**.**

The distance between two foci is = 2c = 15.8-0 =15.8 i.e c=7.9 signifying the center of the Hyperboloid was at (18, 0, 7.9) c is the distance between two foci.

The factual distance, as mentioned, may be calculated, as per section 3.3.3 as

$$f_h = \frac{f_2}{f_1 + f_2}$$

$$\frac{15.8}{2.2 + 15.8}$$

$$0.88$$

As per established literature the acceptable f_h is between 0.5 and 1 [16]. The rays, following the geometry of hyperboloid, were directed to the aim point i.e upper focal point. The passage was truncated by the hyperboloid surface and thus the rays reaches the lower focal point resembling the receiver.

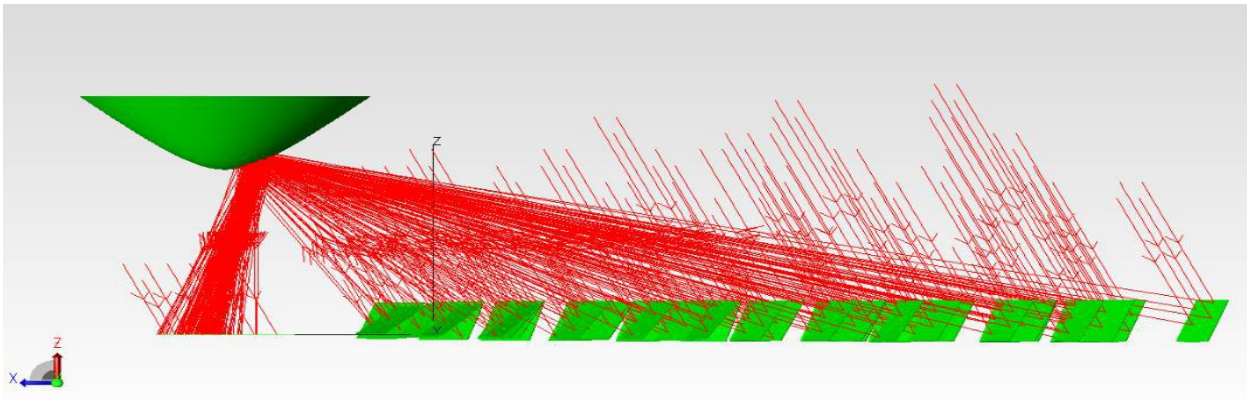

Fig 4.27: Ray tracing with Hyperboloid as secondary reflector

The above figure is a simulation-wise exercise of ray tracing for the purpose. Geometry, as mentioned in section 3.3.3 was followed. The simulation was done for 27th of all the month. From 0900 hrs in the morning to 1700 hrs in the evening was considered at an interval of one hour. The figure below is the ray traced data for 108 cases as mentioned.

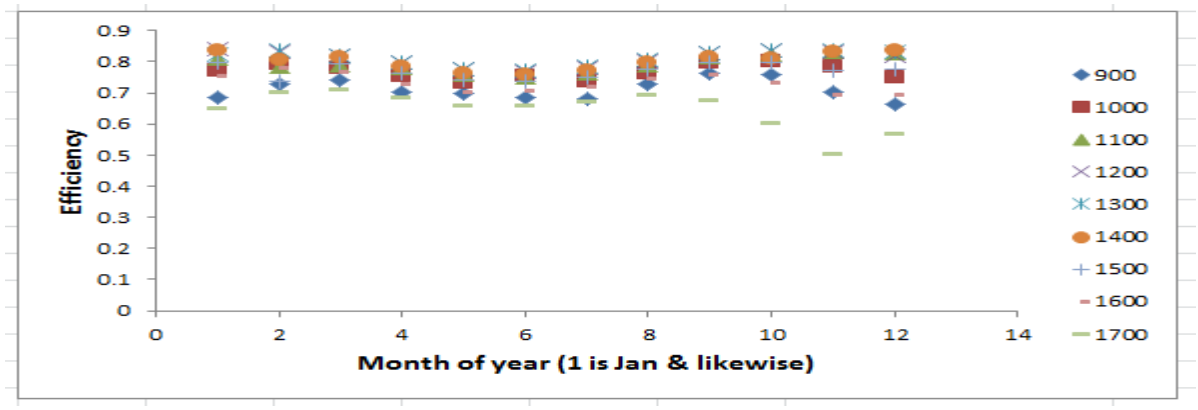

Fig 4.28Ray wise efficiency of the beam down with hyperboloid as secondary

The size of the receiver on the ground was kept at 6 m x 6 m = 36 m^2.

As in figure, half of the one-sheet hyperboloid does not play any productive part and was discarded in this design.

Solar radiation was obstructed with an element of substantial size and in position as it was done in case of use of linear inclined plane as secondary.

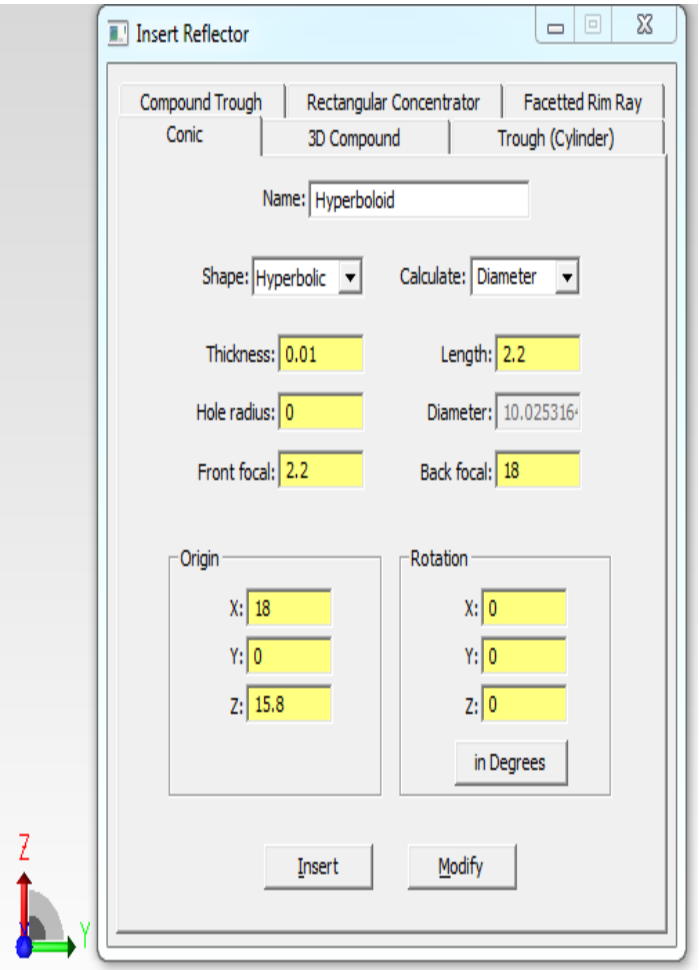

Fig 4.29: Hyperboloid credentials entered in TracePro software

In the above design the Length is the depth of the Hyperboloid opening from the origin (vertex) and diameter is the diameter (system generated) of the circle of the hyperboloid expansion accordingly as per Eq.12.5.The origin of the design was considered as top vertex (18.0.15.8) and back focal point was taken as (18,0,18).That made the top focal point as 2.2 and the top focal point i.e z = 2.2 was the aim point of the Heliostats. The bottom focal point (Front focal in design) was made at z = 2.2 and the bottom vertex was made at (18,0,0).The bottom focal point was the receiver position [16] and the calculation were maintained and shown below.

As mentioned, the conic section expands the size of the beam as it thickens move towards the lower focal point i.e the receiver. In that context, the magnification is relevant as follows

$$M = \frac{f_2}{f_1} = \frac{15.8}{2.2} = 7.18$$

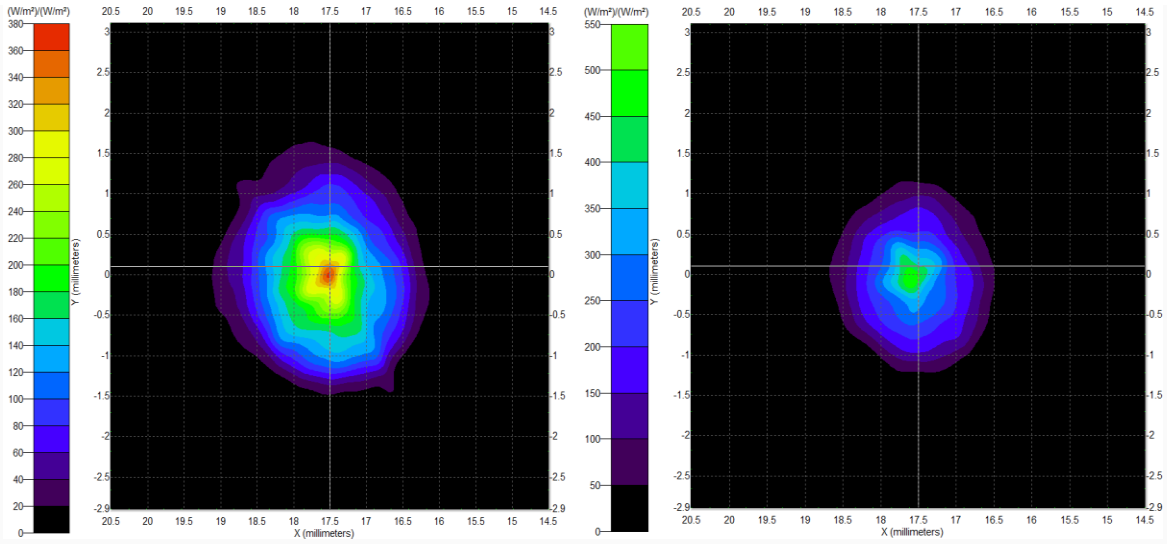

Fig 4.30 Flux mapping for 2703 1200 hrs (left) and 2709 1200 hrs (right)

4.3.3 Ellipsoid as a secondary reflector

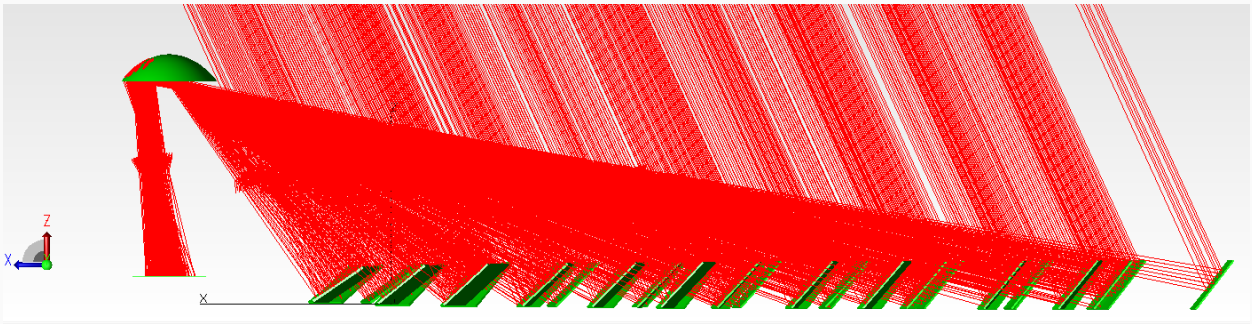

Fig 4.31: Ray tracing with Ellipsoid as secondary reflector

The Ellipsoid geometry (ref section 3.3.4) as a secondary reflector [99,101,103] was introduced in the beam down optics operation of work, which is identical to the Hyperboloid and generates a broad focus. As was understood from the literature [16] and was verified from comparative study in the later sub-section under simulation, this configuration worked with less efficiency than Hyperboloid.

Date and time		Ellipsoid as secondary	
		Ray efficiency	Flux efficiency
2703	900	0.627	0.595
	1200	0.768	0.729
	1700	0.592	0.562
2709	900	0.634	0.601
	1200	0.755	0.717
	1700	0.598	0.51

Table 4.13: Ray and flux wise efficiency for the mentioned date and date using Ellipsoid as secondary reflector.

The lower focal length i.e the position of Receiver was kept at 2.2 above the reference level and the upper focal point (i.e the aim point otherwise in case there is no conic structure).

The size of the receiver on the ground was kept at 6 x 6 = 36 m^2

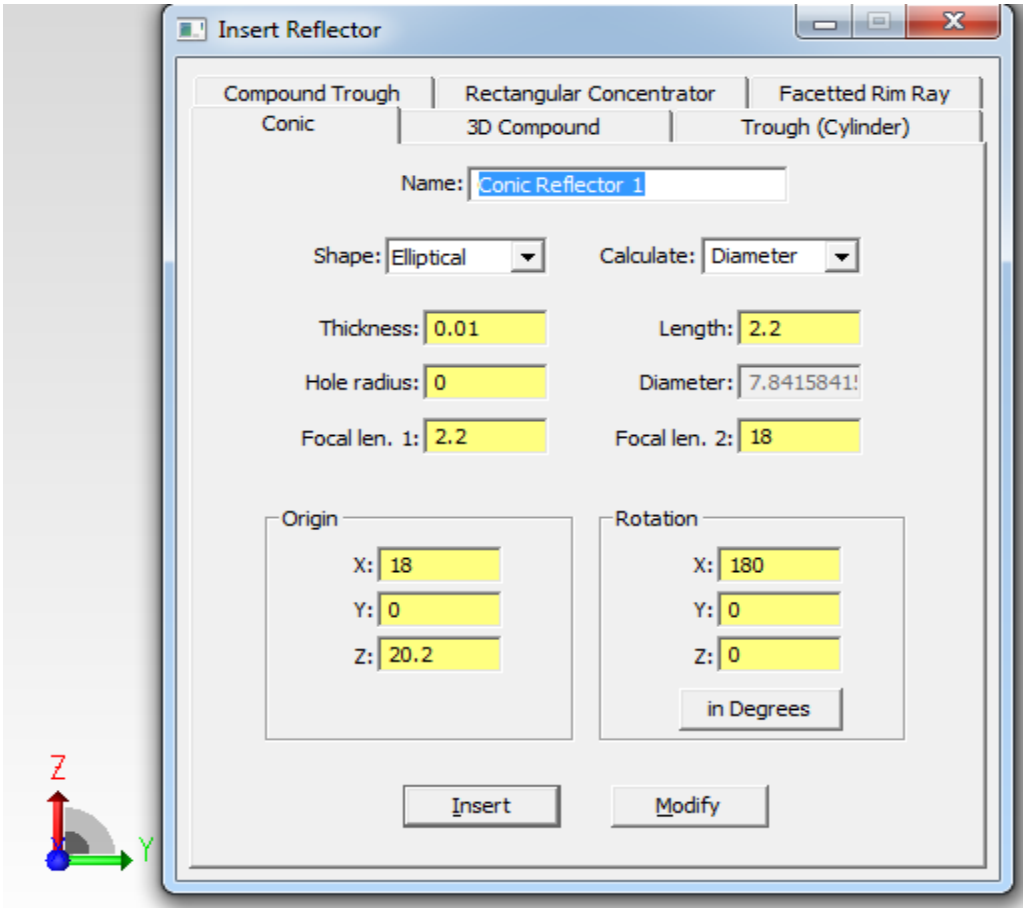

Fig 4.32: Ellipsoid credentials entered in TracePro software

In the above fig. the ellipsoid designed for purpose of work is shown. The origin of the design (18,0,20.2) was the top vertex and focal length 2 at z = 18 was the top focal point i.e the target point for the Heliostats. That made the top focal distance to be 2.2.To make the bottom focal distance to be 2.2 (ellipsoid design condition),the bottom vertex was kept at (18,0,0) and the bottom focal point i.e focal length 1 was made at z = 2.2.**The bottom focal point was the receiver position for the Beam down design .**

4.3.4 Use of CPC together with conic geometry for Beam Down work

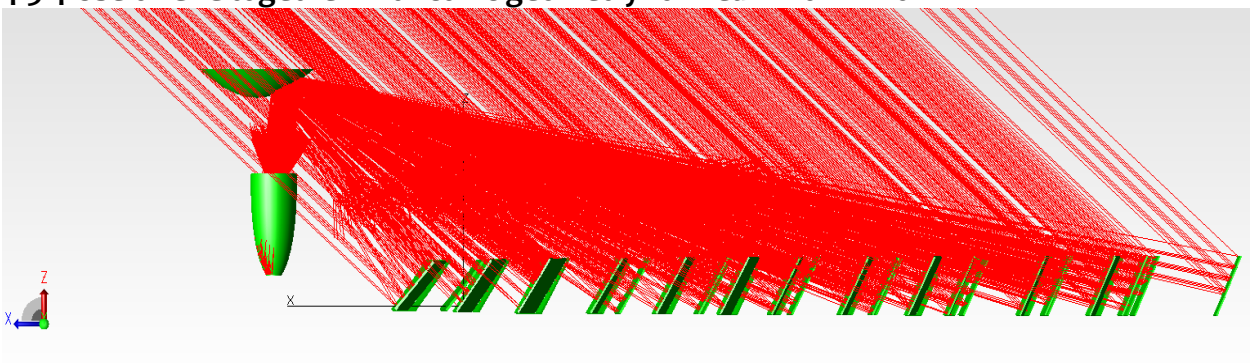

Fig 4.33 : Beam Down work with Hyperboloid and CPC

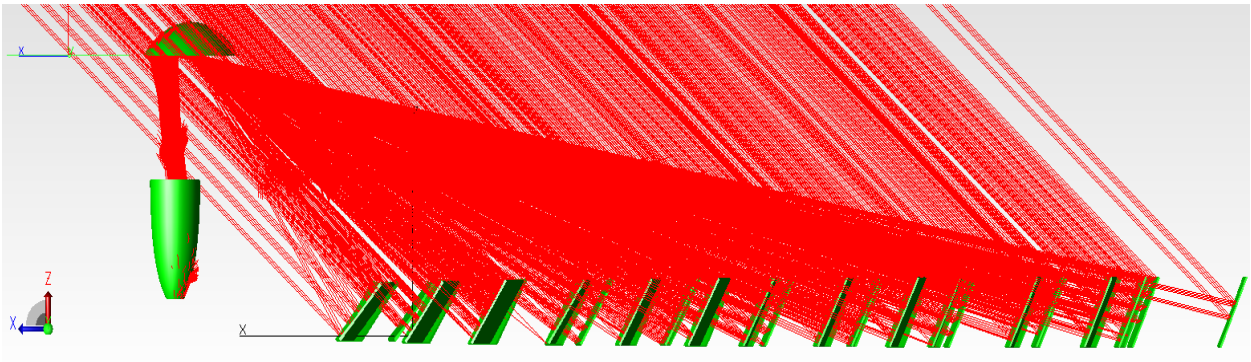

Fig 4.34 : Beam Down work with Ellipsoid and CPC

In Fig 4.33 and 4.34, CPC was used to compensate for the losses due to spread of focal spot on the receiver. The following factors were used for design of the CPC, as per the design tool, Front length = 7.6, Back length = 0, Entry radius = 2 , Exit radius =0.66, Axis tilt =19.27, focal length (as per Eq.12.4) = 0.88, Lateral focal shift (as per Eq 12.5) = Exit radius = 0.66 [83]
The CPC was designed as per mathematics provided and accordingly as per the provisions of the software used. The following is a sample dialog box used for the design in this regard

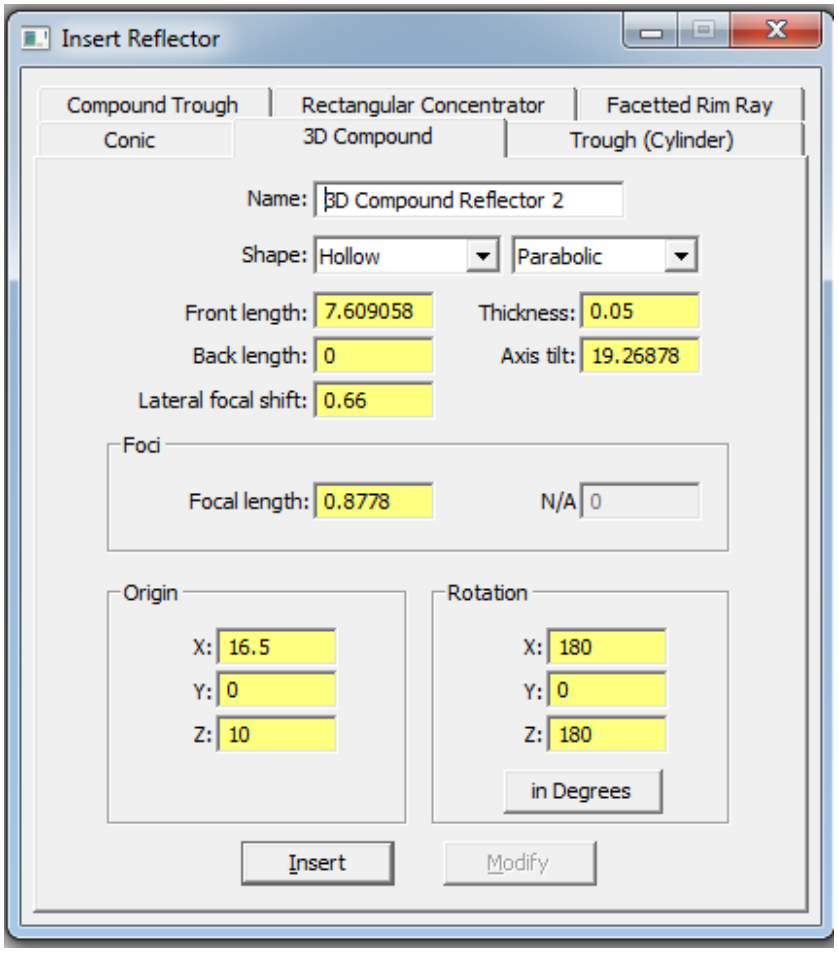

Fig 4.35: Software dialog box for design of concerned CPC

Following are the relevant details of the dialog box [13,83,117]

1 Rotation and origin was given to match the plane setup as per the field design.
2 Front length is equal to length of the CPC (as per calculation)
3 Back length is as per manual.
4. Axis tilt is equal to aperture angle is as per the entrance and exit pupil (user defined value)
5. Lateral Focal Shift is equal to exit pupil radius [83]
6. Focal length is as per manual and literature.

The concentration in this case would remain almost the same in both the case with the following advantages with the CPC because of much smaller size of the receiver under the CPC

1. The radiative losses from the receiver would do down
2. Other than ambient losses, Convective losses go down due to smaller size of receiver
3. Complications regarding the alignment and maintenance would go down.
4. Manufacturing losses and hence the cost would go down.

The Concentration ration, C , in this work for the CPC is as follows

$$C = \frac{Collectoinarea}{Receiverarea} = \frac{1000}{1.37} = 730$$

Fig 4.49 below show a set of data of normalized ray efficiency for the mentioned work

Date	Time (hrs)	Ellipsoid as secondary		Hyperboloid as secondary	
		With CPC	Without CPC	With CPC	Without CPC
	900	0.619	0.624	0.579	0.638
	1000	0.689	0.696	0.731	0.735
	1100	0.788	0.771	0.789	0.79
	1200	0.784	0.804	0.801	0.893
	1300	0.815	0.826	0.819	0.833
	1400	0.804	0.827	0.724	0.752
	1500	0.756	0.767	0.761	0.647
	1600	0.518	0.627	0.584	0.524
2712	1700	0.461	0.514	0.483	0.483

Table 4.14 :A study on difference between two beam down geometry with and without the CPC in respect to normalized ray efficiency

4.4 Comparative study

In this work multiple comparison between configures of work and also manner display of result. A set of those comparisons are tabled below

4.4.1 Study and comparison of Heliostat field design performance for beam up and beam down as mentioned accordingly

Time	0900 hr				1200 hr				1600 hr			
Date	2703	2706	2709	2712	2703	2706	2709	2712	2703	2706	2709	2712
RS Bean Down with curved Heliostats and inclined plane	0.601	0.556	0.611	0.516	0.631	0.599	0.601	0.643	0.605	0.569	0.606	0.529
RS Beam Up with flat Heliostat	0.582	0.545	0.601	0.522	0.639	0.613	0.657	0.646	0.588	0.562	0.603	0.545
Cornfield beam up with curved Heliostats	0.578	0.544	0.582	0.537	0.617	0.611	0.618	0.611	0.585	0.56	0.561	0.565
RS Bean Up with curved Heliostats	0.635	0.589	0.643	0.573	0.691	0.648	0.689	0.7	0.681	0.597	0.649	0.596

Table 4.15: The above table presents twelve (12) configurations for four different setups.

In Table 4.15 above, all data presented with reflectance from all the reflective element of the field, considering beam down and beam up [152]. For the sake of useful calculation, reflectance was taken as 85 %. For the calculation of formidable values for beam down with Inclined plane as secondary reflector, twice the reflectance of 85 % was considered. As mentioned in some cases, June is the worst performing month.

For any day and time, RS field design with flat reflectors may be considered as the worst performer in the above study.

4.4.2 Comparison of optical efficiency over four Heliostat sizes

As mentioned in section 4.2.4,the solar concentration work may be used for power generation in a power plant only when an high assurance and predictability of expected concentration and hence temperature is calculated and predictably known [147, 153]. To that effect, for any time of any day a stagnant temperature is calculated as below

$$T = \left\{\frac{CI}{\sigma}\right\}^{0.25}$$

C in the above equation is the concentration at a particular time and date**, I** is the dni for that particular time and date and **σ** is Stefan Boltzmann constant

Day Considered	Time considered	100 kW with curved Heliostats	400 kW with curved Heliostats	500 kW with curved Heliostats	1.4 MW with curved Heliostats
	900	0.75	0.65	0.65	0.6
	1000	0.87	0.75	0.75	0.71
	1100	0.94	0.83	0.83	0.78
	1200	0.96	0.85	0.84	0.81
	1300	0.92	0.84	0.84	0.8
	1400	0.91	0.79	0.78	0.75
	1500	0.91	0.71	0.71	0.68
	1600	0.77	0.67	0.69	0.63
2712	1700	0.66	0.55	0.56	0.45

Table 4.16: Ray wise Concentration of the four configuration of work.

Day considered	Time considered	Generated Power	Ray efficiency	Stagnant Temperature (K)
	1200	100 kW	0.94	358.83
		400 kW	0.85	349.91
		550 kW	0.85	368.02
2712		1.4 MW	0.81	345.72

Table 4.17: Stagnant temperature calculation

Fig 4.52 show the stagnant temperature obtained from four sizes of Heliostat considered. The stagnant temperature may not be exact because of multiple geographical and other reasons. This temperature was calculated on the basis of efficiency and DNI [70] values from literature.

4.4.3 Comparison between Hyperboloid and Ellipsoid field efficiency for the work as Beam Down was done for twelve chosen cases

Day Considered	Time Considered	Flux wise efficiemcy		Ray wise efficiency		Cosine efficiency	Normalized Blocking and Shadowing efficiency	
		Hyperboloid	Ellipsoid	Hyperboloid	Ellipsoid		Hyperboloid	Ellipsoid
	900	0.622	0.597	0.765	0.627	0.8	0.957	0.784
	1200	0.735	0.729	0.817	0.768	0.89	0.918	0.632
2703	1700	0.557	0.517	0.622	0.548	0.77	0.808	0.712
	900	0.474	0.44	0.53	0.468	0.72	0.736	0.65
	1200	0.682	0.699	0.758	0.739	0.81	0.936	0.912
2706	1700	0.402	0.348	0.451	0.391	0.69	0.654	0.566
	900	0.651	0.549	0.729	0.634	0.87	0.837	0.726
	1200	0.744	0.716	0.827	0.755	0.95	0.87	0.795
2709	1700	0.532	0.507	0.593	0.538	0.84	0.706	0.64
	900	0.574	0.551	0.638	0.624	0.83	0.768	0.751
	1200	0.741	0.756	0.825	0.804	0.91	0.904	0.883
2712	1700	0.471	0.467	0.524	0.514	0.78	0.672	0.659

Table 4.18: Tradeoff between two geometric structures for Beam Down

Receiver size	6 x 6
Rays launched	100 per unit sq

As mentioned in section 4.3.3, all factors of consideration remaining identical, Hyperboloid performs better than the Ellipsoid for solar energy inception and accordingly power generation.

4.4.4 Efficiency Comparison on the basis of Heliostats size

This work involved the use of Heliostats of various sizes.Fig.4.32 show a comparative study of the efficiency of all the curved and tilted Heliostats.

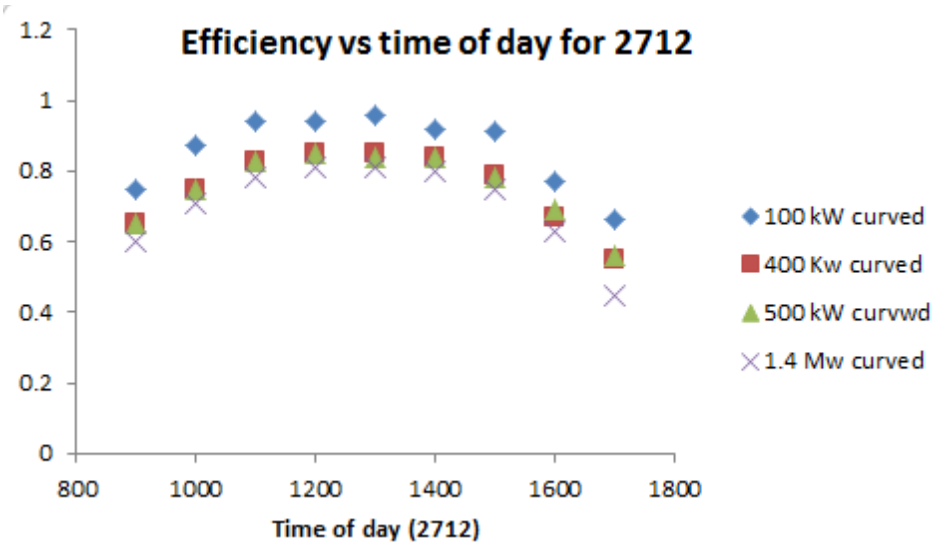

Fig 4.36 : Ray efficiency of the four configuration of work with target power generation.

As shown in figure 4.54, this study was done for entire day of 2712 with nine hours of operation. In all the cases it was found and thus may be concluded that as the size of Heliostats increase, every other thing kept constant, the efficiency decrease. Apart from spillage, as the size of Heliostats increase, the Spherical aberration plays a part on aberration and hence loss of efficiency. As for perfect focusing, the receiver should be at the calculated focal point of the rays from the Heliostat, as the size of Heliostat increases, the axial position of the focal point change. That disturbs the perfect focusing and hence broadens the focal spot [78].

4.4.6 Comparison between RS and SF field design

As a comparative study between SF and RS field design [110] the field design in tern of power generated was calculated and shown in next page

Day Considered	Time considered	Ray wise efficiency		Avg DNI over working hrs (W/m^2)	SF - RS power (kW)in term of normalized ray efficiency
		SF	RS		
2703	900	0.744	0.708	343.6	12.18
	1200	0.843	0.818		8.84
	1700	0.717	0.71		2.56
2706	900	0.782	0.669	364.23	40.86
	1200	0.844	0.768		27.34
	1700	0.756	0.661		34.35
2709	900	0.758	0.72	502.67	19.19
	1200	0.841	0.827		7.23
	1700	0.715	0.675		20.06
2712	900	0.712	0.647	644.29	41.48
	1200	0.9	0.848		33.35
	1700	0.66	0.562		60.85

Table 4.19 : Comparative study between SF and RS power generation

As shown, the SF design has a consistently higher power generation which is maximum in the month of July and December (Solstice time). The increase in power generation in the Equinox time is considerable, but if the year wise calculation is made, keeping every other factor as a constant, SF may be considered as a better power generator.

4.4.5 Comparative study of the various Heliostat layout and various features of design

In this work, multiple field design patterns were done with special focus of Radial Staggered Pattern because of the obvious advantages, regarding reducing the Blocking and Shadowing effect. Table 4.20 gives a gist of all the type of field design simulated and related receiver and other paraphernalia details. The values presented in the column five of the table 4.20, i.e. power on the receiver (approximately) was obtained by considering DNI = 940 W/m^2, employed area of heliostats (mirror area) and normalized ray tracing efficiency.

Layout Type	Heliostat Size	Number of Heliostat on field	Heliostat Surface type	Power on Receiver (approx.)	Receivertype	Receiver size (sqm)	Rim angle on ground	Field size (sqm)
Radial Staggered	2 x 2	181	Curved	600 kW	Cavity Shaped	21	9.25	4074
	2.5 x 2.5	50	Curved	100 Kw	Flat plate	2.25	10.75	1158.69
	4 x 4	50	Flat	400 Kw	Flat plate	25	12.8	2312.59
	5 x 5	40	Flat	550 Kw	Flat plate	16	14.62	2889.3
	8 x 8	40	Curved	1.4MW	Flat plate	4	16.62	6255.53
	5 x 5	181	Curved	3.16 MW	Cavity Shaped	140	12.8	16079
Cornfield	5 x 5	40	Curved	550	Flat plate	4	Not relevant	2084
Sunflower	5 x 5	40	Curved	600	Cylindrical	50.24	Not relevant	4968

Table 4.20: Heliostat layout and various features of design

In this work various field design were made and accordingly multiple receivers were also simulated. As shown in this chapter, the ray efficiency with the Cavity shaped and cylindrical receiver is higher. But bigger size increases the mechanical stress in both cases.

Another noted case was that, especially in Sunflower field design (Fermat's Spiral), the field size to reflective area size ratio was 4.2 with majority of the field lying vacant. Although the advantages of Sunflower design as mention prior in this work, but this turns out to be a disadvantage of the work. It is proposed to generate a hybrid Solar field in this regards to fully utilize the field and compensate the disadvantage.

Tables A.8 in the appendix section is a continuation as a detailed elaboration of the Ray tracing work done in chapter 4